



Extracellular vesicles hybrid plasmid-loaded lipid nanovesicles for synergistic cancer immunotherapy

Qing Tong^{a,b,1}, Kexin Li^{a,b,1}, Fanwei Huang^{a,b}, Yun Dai^{a,b}, Tao Zhang^{a,b},
Munawaer Muaibati^{a,b}, Abasi Abuduyilimu^{a,b}, Xiaoyuan Huang^{a,b,*}

^a National Clinical Research Center for Obstetrics and Gynecology, Cancer Biology Research Center (Key Laboratory of the Ministry of Education), Tongji Hospital, Tongji Medical College, Huazhong University of Science and Technology, Wuhan, China

^b Department of Gynecological Oncology, Tongji Hospital, Tongji Medical College, Huazhong University of Science and Technology, Wuhan, China

ARTICLE INFO

Keywords:

Cancer vaccine
Extracellular vesicles
Liposomes
Hybrid lipid nanovesicles
Akkermansia muciniphila
Immune checkpoint blockade

ABSTRACT

Combination immunotherapy of cancer vaccines with immune checkpoint inhibitors (ICIs) represents a promising therapeutic strategy for immunosuppressed and cold tumors. However, this strategy still faces challenges, including the limited therapeutic efficacy of cancer vaccines and immune-related adverse events associated with systematic delivery of ICIs. Herein, we demonstrate the antitumor immune response induced by outer membrane vesicle from *Akkermansia muciniphila* (Akk-OMV), which exhibits a favorable safety profile, highlighting the potential application as a natural and biocompatible self-adjuncting vesicle. Utilizing tumor cell-derived exosome as an antigen source and Akk-OMV as a natural adjuvant, we construct a cancer vaccine formulation of extracellular vesicles hybrid lipid nanovesicles (Lipo@HEV) for enhanced prophylactic and therapeutic vaccination by promoting dendritic cell (DC) maturation in lymph node and activating cytotoxic T cell (CTL) response. The Lipo@HEV is further loaded with plasmid to enable gene therapy-mediated PD-L1 blockade upon peritumoral injection. Meanwhile, it penetrates into lymph node to initiate DC maturation and CTL activation, synergistically inhibiting the established tumor. The fabrication of extracellular vesicles hybrid plasmid-loaded lipid nanovesicles reveals a promising gene therapy-guided and vesicle-based hybrid system for therapeutic cancer vaccination and synergistic immunotherapy strategy.

1. Introduction

Among the tremendous efforts focused on immunotherapy to facilitate the host immune system in efficiently recognizing and killing tumor cells, cancer vaccines have undergone a resurgence over the past decade [1], evidenced by the tumor-specific immunogenicity and clinical efficacy towards melanoma, glioblastoma and other cancers [2,3]. The basic principles of successful therapeutic vaccination involve delivery of high-quality antigens to dendritic cells (DCs), optimal DC activation, induction of robust and sustained cytotoxic T lymphocyte (CTL) responses, infiltration of the tumor microenvironment (TME) and durability of responses [4], which can be achieved by co-administration of tumor antigens with adjuvants [5], and reversal of tumor-induced immune exhaustion by immune checkpoint blockade [6]. However, conventional cancer vaccines typically show limited therapeutic efficacy in clinical trials due to central and peripheral tolerance responses and elicit

individual varying degrees of immune responses [7]. Moreover, systemic delivery of immune checkpoint inhibitors (ICIs) can cause a series of side effects, including immune-related adverse events (irAEs) and chronic immune toxicity [8–10]. Thus, the precise therapeutic cancer vaccines and rational combination immunotherapies that induce the safe and robust antigen-specific immune responses warrant further development.

Extracellular vesicles (EVs), secreted by both eukaryotic and prokaryotic cells, are a heterogeneous group of lipid-bound nano-sized membrane vesicles that contain hundreds of lipids, proteins, carbohydrates and nucleic acids, and serve as key mediators of various (patho) physiological processes [11]. Tumor-derived EVs, which carry large quantities of cell components originated from the parent tumor cells, can be exploited as a tumor antigen source in a non-replicative form [12]. On the other hand, the gut microbiota has been demonstrated as both a biomarker and an adjuvant for enhancing clinical response to ICIs [13].

* Corresponding author Tongji Hospital, Tongji Medical College, Huazhong University of Science and Technology; 1095 Jiefang Avenue. Wuhan, 430030, China.
E-mail address: huangxy@tjh.tjmu.edu.cn (X. Huang).

¹ Qing Tong and Kexin Li contributed equally to this work.

Akkermansia muciniphila, a gram-negative bacterium as the paradigm for next-generation beneficial microorganisms, is a promising candidate to enhance the clinical response to checkpoint inhibitor immunotherapies [14–16]. Clinical trials are crucial to confirm the role of *Akkermansia muciniphila* in increasing the success of immunotherapies, whereas further studies are needed for a deeper understanding of the mode of action [17]. Recent studies have shown that *Akkermansia muciniphila* and its secreted protein 9 (P9) stimulate the secretion of IL-6 by macrophages and enterocytes [18], and the outer membrane protein Amuc-1100 blunts colitis associated tumorigenesis by modulation of CD8⁺ T cells in mice [19]. Utilizing spectroscopic analysis and chemical synthesis instead of multi-omics technique, a newly identified PE lipid from *Akkermansia muciniphila* has been demonstrated to promote the release of TNF- α and IL-6 in DCs [20]. Given that bacterial extracellular vesicles (BEVs) are nanometer-scale packages of adjuvant components inherited from the parent bacteria [21–23], we hypothesize that the outer membrane vesicle from *Akkermansia muciniphila* (Akk-OMV) mediates the enhancement of the parent bacterium to checkpoint inhibitor immunotherapy, and can be further exploited as a natural nanoadjuvant for therapeutic cancer vaccination.

Herein, we purified three kinds of BEVs by means of differential centrifugation with size exclusion chromatography method, and demonstrated the antitumor immune response of Akk-OMV that prevented tumorigenesis and synergized with PD-L1 antibody against tumor growth. Upon different regimes of subcutaneous and intraperitoneal injections, Akk-OMV exhibited a favorable safety profile, which was suitable for further adjuvant immunotherapy strategies. Taking advantage of vesicle fusion technique that potentiated the hybrid vesicles with properties inherited from different mono-vesicles [24,25], the cancer vaccine formulation of EVs hybrid lipid nanovesicles (Lipo@HEV) was fabricated for co-delivery of antigens from tumor cell-derived exosome and adjuvant components from Akk-OMV, enabling the activation of DC maturation and CTL response for enhanced cancer vaccination. The Lipo@HEV based on the co-delivery vector of cationic liposome was further loaded with a PD-L1 trap plasmid to achieve PD-L1 blockade in tumor for reversing CTL exhaustion and avoiding irAEs. Simultaneously, the plasmid-loaded Lipo@HEV penetrated into the lymph nodes to promote DC maturation and activate CTL response, improving the antitumor activity of PD-L1 blockade against the established tumor. The present study demonstrates the synergistically immunotherapeutic potential of the plasmid-loaded extracellular vesicles hybrid lipid nanoplateform, providing an extensible, biomimetic and gene therapy-based approach for therapeutic cancer vaccination and combination immunotherapy.

2. Material and methods

2.1. Cell culture and animals

The murine melanoma cell line B16–F10 and murine breast cancer cell line 4T1 were obtained from American Type Culture Collection (ATCC). DC2.4 cell line was obtained from Procell Life Science & Technology Co. Ltd (Wuhan, China). B16–F10 and CT26 were cultured in DMEM medium (Gibco) with 10 % FBS, and 4T1 and DC2.4 cells were cultured in 1640 medium (Gibco) with 10 % FBS. All the cell lines were incubated at 37 °C with 5 % CO₂, and antibiotics (1 % penicillin/streptomycin, v/v) were added to cell culture medium. Female C57BL/6 and BALB/c mice (6–8 week) were purchased from Vital River Laboratory Animal Technology Co. Ltd (Beijing, China) and maintained under specific pathogen-free (SPF) condition. All animal experiments were conducted under guidelines approved by the Animal Care and Use Committee of Tongji Hospital, Tongji Medical College, Huazhong University of Science and Technology (SYXK 2019-0106).

2.2. Isolation and characterization of EVs

Both eukaryotic and prokaryotic EVs were isolated by differential centrifugation method according to the previous studies with some modifications [26,27]. For isolation of tumor cell-derived exosomes, B16–F10, 4T1 and CT26 tumor cells were cultured in DMEM or 1640 medium with 10 % FBS until 60–70 % density. The cells were washed with PBS, and maintained in Opti-MEM medium (Gibco) for another 48 h. The supernatant was collected and centrifuged at 800 g for 5 min and 2000 g for 10 min at 4 °C. The supernatant was filtered using 0.4 μ m polycarbonate membrane (Millipore), and the pellet was recovered after ultracentrifugation of 200000 g for 70 min at 4 °C. The supernatant was aspirated, and the pellet was resuspended in PBS and subsequently ultracentrifuged at 200000 g for 90 min at 4 °C. For isolation of BEVs, *E. Coli* DH5 α were cultured in LB medium at 37 °C with 250 rpm shaking overnight, and the cultured cells were pelleted at 12000 g for 10 min at 4 °C. The supernatant was filtered using 0.4 μ m polycarbonate membrane (Millipore), and the pellet was recovered after ultracentrifugation of 200000 g for 70 min at 4 °C. The supernatant was aspirated, and the pellet was resuspended in PBS and subsequently ultracentrifuged at 200000 g for 90 min at 4 °C. The collected pellet was purified by a size exclusion filter (Umibio, UR90102). *Akkermansia muciniphila* (ATCC BAA-835) were cultured in the brain heart infusion broth medium (BD BBL, 211059), and *Bifidobacterium pseudolongum* (ATCC 25526) were cultured in the modified reinforced clostridial broth medium (Shandong Tuopu Biol-engineering Co. Ltd., MD039) for 7 days under anaerobic conditions. The medium was supplemented with resazurin (5 mg/L) and L-cysteine (0.5 g/L). The cultured bacteria were pelleted twice at 12000 g for 10 min at 4 °C, and the isolation procedures were the same as those of *E. Coli* DH5 α -OMV. The morphology of exosome and BEVs were imaged by TEM (Hitachi, HT7700) after negative staining with 2 % phosphotungstic acid. The diameter and zeta potential were determined by nanoparticle tracking analysis (NTA, Particle Metrix, Germany). The protein profiles were analyzed by SDS-PAGE with equal loading amounts of 10 μ g vesicle protein, measured by the BCA assay (Beyotime, P0010).

2.3. Prophylactic antitumor evaluation of BEVs and transcriptome sequencing analysis

Akk-OMV, DH5 α -OMV and Bifi-CMV were subcutaneously injected at the tail base of BALB/c mice (10 μ g) at 3 day-intervals for 5 times, respectively, and mice were subcutaneously inoculated with 2×10^5 4T1 tumor cells 7 days after the final injection. The tumor volume was measured every 2 days and calculated according to the formula $V (\text{mm}^3) = \text{length} \times \text{width}^2 \times 0.52$. The maximal tumor burden permitted was 1500 mm^3 . After the prophylactic antitumor evaluation study of different BEVs, the collected spleens and tumors were snap frozen in liquid nitrogen. The total RNA was extracted using Trizol-reagent (Invitrogen) according to the manufacturer's protocol. Then eukaryotic mRNA was enriched by Oligo(dT) beads, and the enriched mRNA was fragmented into short fragments using fragmentation buffer and reverse transcribed into cDNA with random primers. Second strand cDNA were synthesized by DNA polymerase I, RNase H, dNTP and buffer. The cDNA fragments were purified, end repaired, poly(A) added and ligated to Illumina sequencing adapters. The ligation products were size selected by agarose gel electrophoresis, PCR amplified and sequenced using Illumina HiSeq2500. The data were analyzed by the online platform of Majorbio Cloud Platform.

2.4. Antitumor immune response induced by Akk-OMV and combination therapy with PD-L1 antibody

BALB/c mice were subcutaneously inoculated with 2×10^5 4T1 tumor cells on day 0, and Akk-OMV was subcutaneously injected at the tail base (20 μ g) on day 10, 13, 16, 19 and 22. Then mice were

euthanized on day 25, and tumors, lymph nodes and spleens were collected for flow cytometry analysis. For combination therapy of Akk-OMV with PD-L1 antibody, BALB/c mice were subcutaneously inoculated with 2×10^5 4T1 cells on day -8. Akk-OMV was subcutaneously injected at the tail base (20 μ g) on day 0, 3, 6, 9 and 12, and PD-L1 antibody (Leinco Technologies, P363) was intraperitoneally injected (150 μ g) on day 6, 9 and 12. The tumor volume was measured every 3 days and calculated according to the formula $V (\text{mm}^3) = \text{length} \times \text{width}^2 \times 0.52$. The mice were euthanized on day 21, and the tumors and spleens were collected for flow cytometry analysis.

2.5. *In vivo biosafety evaluation of Akk-OMV*

For a single-dose intraperitoneal injection, BALB/c mice were injected with Akk-OMV or DH5 α -OMV at a dose of 20 μ g, and the mice were euthanized at 8 h post-injection. For 3 times intraperitoneal injections, BALB/c mice were injected with Akk-OMV or DH5 α -OMV at a dose of 20 μ g on day 0, 3, 6, and the mice were euthanized on day 14. The survival rate was recorded during the treatments. For 3 times subcutaneous injections, C57BL/6 mice were injected with Akk-OMV or DH5 α -OMV at a dose of 20 μ g on day 0, 3, 6, and the mice were euthanized on day 9. The serum was collected, and hepatic and renal function indexes were evaluated by Chemray240 biochemical auto-analyzer. The major organs including hearts, livers, spleens, lungs and kidneys were collected, and H&E staining was conducted to evaluate the organ histological changes.

2.6. *Preparation of EVs hybrid lipid nanovesicles*

The cationic liposome was prepared via thin-film hydration method. DOTAP (Avanti Polar Lipids, 890890P) and cholesterol (Sigma, 700000P) were dissolved in chloroform at a molar ratio of 1:1, and the solvent was evaporated under nitrogen flow. The dry film was hydrated with ultra-pure water by magnetic stirring overnight to obtain a coarse suspension with stock concentration of 10 mM each. The obtained suspension was extruded 11 times through polycarbonate membranes of 800 nm, 400 nm and 200 nm using a mini-extruder (Avanti Polar Lipids). To prepare the EVs hybrid lipid nanovesicles, cationic liposome was mixed with EVs and then sonicated with a probe ultrasonicator (50 % power, 130 W, 20 kHz) for 2 min (2 s interval) in ice water bath. Then the solution was co-extruded at least 5 times through polycarbonate membranes of 800 nm, 400 nm and 200 nm. To prepare plasmid-loaded EVs hybrid lipid nanovesicles, cationic liposome was first incubated with plasmid at N/P ratio of 5 for 15 min, and then sonicated and co-extruded with EVs. The pcDNA3.1 plasmid encoding PD-L1 trap was constructed by VectorBuilder (Guangzhou, China) according to the previous studies [28,29]. For the validation of PD-L1 trap plasmid, the DNA sequencing, restriction enzyme analysis (*Apa*LI and *Fsp*LI) and agarose gel electrophoresis were conducted. The pRP-CMV-Luciferase plasmid was obtained from VectorBuilder (Guangzhou, China). The plasmids were extracted and purified using a EndoFree Maxi Plasmid Kit (Tiangen, China), and the accuracy was validated by DNA sequencing.

2.7. *Characterization of EVs hybrid lipid nanovesicles*

The morphology of exosome, OMV and hybrid nanovesicles were imaged by TEM (Hitachi, HT7700) after negative staining with 2 % phosphotungstic acid. The size and zeta potential were analyzed by NTA. For fusion analysis of EVs with cationic liposome, OMV and exosome were incubated with PKH26 (Sigma, MINI26) and PKH67 (Sigma, MINI67) at final dye concentration of 5 μ M for 10 min, respectively. After ultra-centrifugation at 200000g for 70 min at 4 $^{\circ}$ C, the pellets of dye-labeled exosome and OMV were resuspended in PBS and co-extruded with cationic liposome at different weight ratios of 100:1:1, 50:1:1, 20:1:1. The membrane colocalization was imaged using a confocal laser scanning microscope (CLSM, Nikon Eclipse TI), and

quantified by nano-flow cytometry (NanoFCM). The tumor cell membrane (TCM) was extracted using a membrane and cytosol protein extraction kit (Beyotime, P0033) according to the manufacturer's instructions, and Lipo@HMV was prepared by fusing liposome with OMV and TCM following the same preparation procedure of Lipo@HEV. The protein profile was analyzed by SDS-PAGE, and all the samples were normalized to equivalent protein concentration of 10 μ g measured by the BCA assay (Beyotime, P0010). The gel was stained in Coomassie brilliant blue dye solution (Servicebio, G2059) for 2 h and washed with in ultra-pure water for 4 h, and the gel was imaged by a Bio-Rad ChemiDoc MP Imaging System. For western blot analysis of exosome markers, proteins were transferred to polyvinylidene fluoride (PVDF) membranes, which were blocked with 5 % nonfat milk TBST for 1 h and incubated with primary antibodies of CD9 (Abcam, ab92726) and TSG101 (Abcam, ab125011) overnight at 4 $^{\circ}$ C, followed by washing and incubating with a goat anti-rabbit IgG-HRP secondary antibody (Abcam, ab205718). The blots were imaged by a Bio-Rad ChemiDoc MP Imaging System.

2.8. *In vitro cellular uptake and dendritic cell maturation analysis*

For cytotoxicity assay, B16-F10 and DC2.4 cells were seeded in 96-well plates and incubated with Lipo@HEV at different concentrations of total lipids for 24 h, and the cytotoxicity was determined by CCK8 assay. After PKH26/PKH67 staining of OMV/exosome and hybrid lipid nanovesicles preparation, B16-F10 and DC2.4 cells were seeded on glass coverslips and treated with PKH26/PKH67-labeled Lipo@HEV for 6 h. The cells were fixed with 4 % paraformaldehyde for 20 min and stained with DAPI for 10 min, then imaged by CLSM. BMDCs were differentiated from bone marrow cells isolated from the femurs and tibias of C57BL/6 mice according to the previous method [30]. The cells were cultured in 1640 medium supplemented with 10 % FBS, 20 ng/mL GM-CSF (PeproTech, 315-03) and 10 ng/mL IL-4 (PeproTech, 214-14) in petri dishes. The non-adherent and loosely adherent cells were collected and treated with PKH26/PKH67-labeled Lipo@HEV for 6 h. The cellular uptake rate of PKH26/PKH67-labeled hybrid lipid nanovesicles was quantitative analyzed by flow cytometry (Beckman Coulter CytoFLEX). For DC maturation assay, BMDCs were plated into 24-well non-treated dishes and stimulated with different EVs and formulations of hybrid lipid nanovesicles (3 μ g/mL vesicle protein) for 24 h. Then BMDCs were collected and incubated with anti-CD16/32 (Biolegend, 156603), and stained with FITC-anti-CD11c (Biolegend, 117306), PE-anti-CD80 (Biolegend, 104707) and APC-anti-CD86 (Biolegend, 105011) according to the manufacturer's protocols, followed by flow cytometry analysis. The data were analyzed by CytExpert 2.4 software.

2.9. *In vivo biodistribution and plasmid transfection imaging*

For the biodistribution study of Akk-OMV, the purified Akk-OMV was first labeled with near-infrared fluorescent dye DiR at the concentration of 50 μ M. After 1 h incubation at room temperature, unbound dye was removed by ultra-centrifugation at 200000g for 70 min at 4 $^{\circ}$ C, and the pellet was resuspended in PBS. Then the DiR-labeled Akk-OMV was subcutaneously injected at tail base of BALB/c mice at the dose of 10 μ g. The major organs and inguinal lymph nodes were collected at 24, 36 and 48 h post-injection, and imaged by Caliper Spectrum In-vivo Imaging System. For the biodistribution study of hybrid lipid nanovesicles, DiR-labeled B16-F10 exosome and Akk-OMV were co-extruded with liposome to generate DiR-labeled Lipo@B16-EXO, Lipo@Akk-OMV and Lipo@HEV, and different formulations were subcutaneously injected at the tail base of C57BL/6 mice at the dose of 20 μ g. The major organs and inguinal lymph nodes were collected and imaged at 48 h post-injection. For the biodistribution study of Lipo-PD-L1@HEV upon peritumoral injection, DiR-labeled B16-F10 exosome and Akk-OMV were co-extruded with plasmid-loaded liposome to generate the DiR-labeled Lipo-PD-L1@HEV. Then the DiR-labeled Lipo-PD-L1@HEV

was peritumorally injected to B16–F10 tumor-bearing mice at the dose of 20 µg. The tumors, lymph nodes and major organs were collected and imaged at 48 h post-injection. For in vivo and ex vivo bioluminescence imaging, Lipo-luciferase and Lipo-luciferase@HEV were peritumorally injected into B16–F10 tumor-bearing mice at the dose of 15 µg plasmid, respectively. The mice were anesthetized and imaged at 48 h post-injection after intraperitoneal injection of D-luciferin potassium salt (ST196, Beyotime). Then the tumors and major organs were collected, and the ex vivo imaging were conducted.

2.10. In vivo antitumor evaluation of EVs hybrid lipid nanovesicles

For the prophylactic study of EVs hybrid lipid nanovesicles, C57BL/6 mice were randomly divided into five groups: (1) control, (2) Lipo@B16-EXO, (3) Lipo@Akk-OMV, (4) Lipo@B16-HEV, (5) Lipo@4T1-HEV. The different formulations were subcutaneously injected at the tail base of the mice (40 µg vesicle protein), and the injections were performed at 3 day-interval for 3 times. Seven days after the final injection, mice were subcutaneously inoculated with 2×10^5 B16–F10 cells. For the therapeutic study of EVs hybrid lipid nanovesicles, C57BL/6 or BALB/c mice were randomly divided into four groups: (1) control, (2) Lipo@EXO, (3) Lipo@Akk-OMV, (4) Lipo@HEV. The mice were subcutaneously inoculated with 2×10^5 B16–F10 or CT26 cells on day 0, and the different formulations were subcutaneously injected at the tail base (40 µg vesicle protein) on day 4, 7 and 10. For the therapeutic study of Lipo-PD-L1@HEV, C57BL/6 or BALB/c mice were randomly divided into three groups: (1) control, (2) Lipo-PD-L1, (3) Lipo-PD-L1@HEV. C57BL/6 mice and BALB/c mice were subcutaneously inoculated with 2×10^5 B16–F10 cells or 4T1 tumor cells on day 0, and different formulations were peritumorally injected on day 9 at 3 day-intervals for 3 times with equal dose of 20 µg plasmid. The tumor volume was measured every 2–3 days and calculated according to the formula $V (\text{mm}^3) = \text{length} \times \text{width}^2 \times 0.52$. The maximal tumor burden permitted was 1500 mm³.

2.11. Single-cell RNA-sequencing analysis

After the prophylactic antitumor evaluation of EVs hybrid lipid nanovesicles, the tumors from Lipo@B16-HEV or control group were pooled and stored in the tissue storage solution (Miltenyi Biotec, 130-100-008). The sample preparation and sequencing were conducted by Berry Genomics Co., Ltd. (Beijing, China). The data were processed by 10 × cellranger software to get the basic expression file, cells with fewer than 200 genes or more than 6000 genes detected were removed. Genes that were expressed in fewer than 2 cells were also removed. The principal components were calculated using scanpy.pca. Dimensionality reduction and embedding was performed using UMAP analysis by the scanpy.tl.umap function. Differentially expressed genes were calculated using the Wilcoxon sum rank test with a fold change cutoff of 2. All *p*-values were adjusted for multiple testing using the Bonferroni correction. Initial annotation was ascribed by comparing the defined cell type markers. Pathway enrichment analysis was performed using the ssGSEA function from gseapy package with default parameters. Gene sets were obtained from the MSigDB database (<https://www.gsea-msigdb.org/gsea/msigdb>).

2.12. Flow cytometry analysis

The collected tumors, spleens and lymph nodes were stored in the tissue storage solution, followed by mechanical disruption and filtering through 70 µm cell strainers to obtain the single-cell suspensions. The tumor cells were incubated with anti-CD16/32 (Biolegend, 156603), and stained with APC-anti-CD3 (Biolegend, 100236) and PE-anti-CD8 (Biolegend, 100707), or FITC-anti-CD4 (Biolegend, 100405), APC-anti-CD25 (Biolegend, 102011), and BV421-anti-FOXP3 (Biolegend, 126419). The splenocytes were incubated with anti-CD16/32 (Biolegend, 156603), and stained with APC-anti-CD3 (Biolegend, 100236),

PE-anti-CD8 (Biolegend, 100707), PerCP/Cyanine5.5-anti-CD44 (Biolegend, 103031), and FITC-anti-CD62L (Biolegend, 104405). The lymph node cells were incubated with anti-CD16/32 (Biolegend, 156603), and stained with FITC-anti-CD11c (Biolegend, 117306), APC-anti-CD86 (Biolegend, 105011), and PE-anti-CD80 (Biolegend, 104707), or APC-anti-CD3 (Biolegend, 100236), and PE-anti-CD8 (Biolegend, 100707). The staining procedure was performed according to the manufacturer's protocol, followed by flow cytometry analysis (Beckman Coulter CytoFLEX). The data were analyzed by CytExpert 2.4 software.

2.13. Immunofluorescence analysis

The collected spleens were fixed in 4 % paraformaldehyde, embedded in paraffin and sectioned. After deparaffinization, rehydration, antigen recovery and blocking with 3 % hydrogen peroxide and 5 % BSA, the spleen sections were dual immunofluorescence stained with primary antibodies of CD4 (Servicebio, G15064) and CD8 (Servicebio, G15068) overnight at 4 °C, followed by incubation of Cy3-conjugated (Servicebio, GB21303) and FITC-conjugated secondary antibodies (Servicebio, GB22303) at room temperature for 1 h, respectively. Mounting was performed using a fluormount containing DAPI (Servicebio, G1407) for further image acquisition (Olympus BX53).

2.14. Enzyme-linked immunosorbent assay of serum cytokines

The blood samples were collected from mice and stored at 4 °C overnight to obtain the serum samples after centrifugation at 8000g for 15 min. The serum samples were stored at –80 °C until further analysis. The concentrations of TNF-α (Invitrogen, 88-7324-22), IL-6 (Invitrogen, 88-7064-22), and IFN-γ (MultiSciences, EK280/3-48) were analyzed by enzyme-linked immunosorbent assay (ELISA) according to the instructions of the ELISA kits.

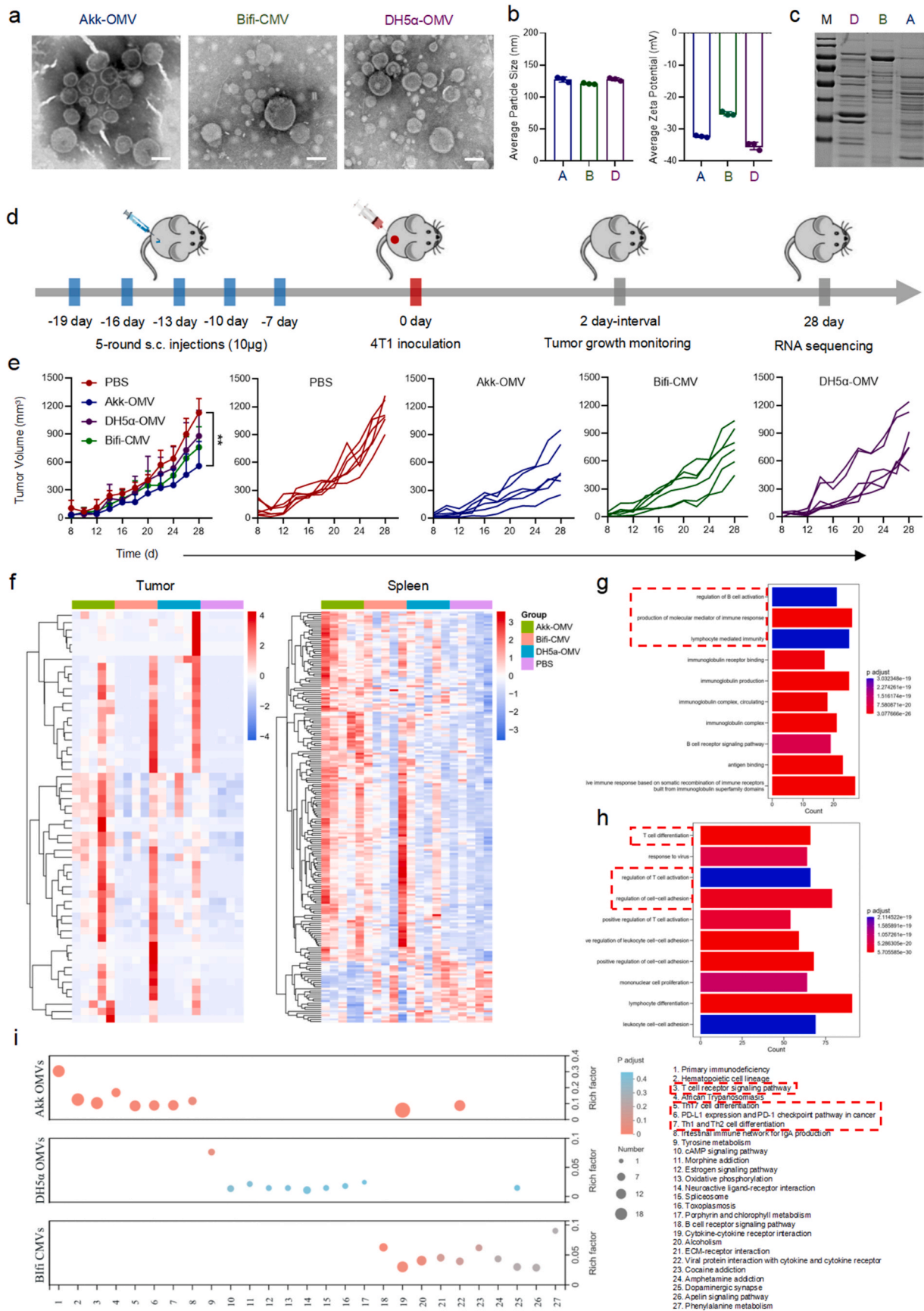
2.15. Statistical analysis

Data analysis was conducted by Graphpad Prism 8.0 software. One-way ANOVA post hoc Tukey multiple comparison test was used for comparisons of more two groups, and student's *t*-test was used for comparisons between two groups. Graphs included means and error bars with all results presented as mean ± standard deviation (SD) or standard error of mean (SEM) as indicated in the figure legends. For survival rate study, log-rank (Mantel-Cox) test was used. The statistically significant was considered as follows: **p* < 0.05, ***p* < 0.01, ****p* < 0.001.

3. Results and discussion

3.1. Antitumor immune response induced by Akk-OMV

Given the anaerobic characteristic of *Akkermansia muciniphila*, the culturing procedure was conducted under the strict anaerobic conditions with mucin-based brain heart infusion broth (BHI) medium. However, the transmission electron micrograph (TEM) images showed the impurity of Akk-OMV after bacterial culturing in mucin-based BHI medium or differential centrifugation without further purification process (Fig. S1). After optimization of culture condition and purification procedure, the differential centrifugation with size exclusion chromatography method was utilized to isolate the OMVs from gram-negative bacteria *Akkermansia muciniphila* and *Escherichia coli* DH5α (DH5α-OMV), and cytoplasmic membrane vesicle from gram-positive bacterium *Bifidobacterium pseudolongum* (Bifi-CMV). TEM images indicated that Akk-OMV, Bifi-CMV and DH5α-OMV displayed nano-sized lipid-bilayer vesicular structures (Fig. 1a), with average diameters of 127.5 ± 4.9 nm, 141.9 ± 2.3 nm and 127.8 ± 2.3 nm, and average zeta potentials of -44.73 ± 1.71 mV, -25.19 ± 0.61 mV and -35.11 ± 1.69 mV, respectively, as measured by nanoparticle tracking analysis (NTA) (Fig. 1b). The SDS-PAGE analysis was conducted to evaluate the protein



(caption on next page)

Fig. 1. Characterization of BEVs and antitumor vaccination efficacy of Akk-OMV. (a) TEM images of BEVs (scale bar: 100 nm). (b) Average particle sizes and zeta potentials of BEVs (A, Akk-OMV; B, Bifi-CMV; D, DH5 α -OMV) measured by nanoparticle tracking analysis (n = 3). (c) SDS-PAGE analysis of protein components in BEVs (M, Marker; A, Akk-OMV; B, Bifi-CMV; D, DH5 α -OMV). (d) Experimental design: BALB/c mice were subcutaneously injected at the tail base with PBS, Akk-OMV, Bifi-CMV or DH5 α -OMV (10 μ g) at 3 day-intervals for 5 times, and then inoculated with 2×10^5 4T1 tumor cells on day 0. Mice were euthanized on day 28 for RNA-sequencing analysis. (e) Tumor growth kinetics after vaccination of different BEVs (n = 6). (f) Transcriptome heatmap of DEGs in tumors and spleens of mice vaccinated with different BEVs and PBS (n = 5). GO pathway enrichment analysis in (g) tumors and (h) spleens of Akk-OMV versus the PBS control. (i) KEGG pathway enrichment analysis in spleens in Akk-OMV, Bifi-OMV and DH5 α -OMV compared to the PBS control. Data are presented as mean \pm SD. Statistical significance was calculated via one-way ANOVA with Tukey multiple comparisons test. **p < 0.01 versus corresponding control group.

profile of three kinds of BEVs, and the results indicated the obvious different protein components originated from the parent bacteria (Fig. 1c).

To investigate the prophylactic vaccination capacity of different BEVs, Akk-OMV, Bifi-CMV and DH5 α -OMV were subcutaneously injected to BALB/c mice at 3 day-intervals for 5 times before 4T1 tumor inoculation (Fig. 1d). Akk-OMV vaccination significantly alleviated the tumor growth, while the effects of Bifi-CMV and DH5 α -OMV were not obvious, which indicated the durable tumor-preventing capacity of Akk-OMV (Fig. 1e). We next conducted RNA-sequencing to profile the differentially expressed genes (DEGs) in the transcriptomes of tumors and spleens from vaccinated mice. The DEGs analysis showed that BEVs vaccination altered various gene expressions in spleens and tumors compared to PBS control, of which Akk-OMV caused the most pronounced changes (Figs. S2a–d, and Figs. S3a–d). Kyoto Encyclopedia of Genes and Genomes (KEGG) annotation analysis revealed that the DEGs in spleens and tumors caused by Akk-OMV vaccination were mainly categorized in the immune system (Fig. S2e, and Fig. S3e). According to the gene expression heatmap in tumors and spleens among different groups (Fig. 1f) and corresponding Gene Ontology (GO) pathway enrichment analysis, the tumors with Akk-OMV vaccination revealed the important role of major pathways such as regulation of B cell activation, production of molecular mediator of immune response and lymphocyte mediated immunity (Fig. 1g), and DEGs in Akk-OMV vaccinated spleens were enriched in the major pathways including T cell differentiation, regulation of T cell activation and regulation of cell-cell adhesion (Fig. 1h). In addition, KEGG pathway enrichment analysis of splenic DEGs indicated the predominant role of immune-related pathways after Akk-OMV vaccination, including T cell receptor signaling pathway, Th17 cell differentiation, Th1 and Th2 cell differentiation, and PD-L1 expression and PD-1 checkpoint pathway in cancer (Fig. 1i). Collectively, these transcriptome analysis results explained the immunomodulatory effect of Akk-OMV vaccination, which lastly exhibited the tumor-preventing capacity.

To verify the antitumor immune response induced by Akk-OMV, the near-infrared fluorescent dye DiR-labeled Akk-OMV was subcutaneously injected at the tail base of BALB/c mice, and the fluorescence signals of major organs indicated that Akk-OMV was mainly distributed in liver as analyzed by the In-vivo Imaging System (IVIS). In addition, the signals of inguinal lymph nodes were observed at different time points of 24, 36 and 48 h, revealing the migration and retention of Akk-OMV into lymph node (Figs. S4a–c). We next performed 5-round subcutaneous injection of Akk-OMV to BALB/c mice after 4T1 tumor inoculation (Fig. S5a). Flow cytometry analysis proved that Akk-OMV treatment promoted the expression of maturation markers on DCs (CD80⁺CD86⁺ in CD11c⁺) in lymph node (Fig. S5b). Moreover, Akk-OMV treatment caused a significant increase of CTLs (CD8⁺ in CD3⁺) and effector memory T cells (T_{EM}, CD44⁺CD62L⁻ in CD3⁺CD8⁺) in splenocytes (Figs. S5c–d), and intratumoral infiltration of CTLs was upregulated as well (Fig. S5e). Given the robust association of *Akkermansia muciniphila* with favorable antitumor responses of ICI [14–17], we further investigated the mediating role of Akk-OMV in the enhancement of parent bacterium to checkpoint inhibitor immunotherapies. 5-round subcutaneous injection of Akk-OMV in 4T1 tumor-bearing mice on day 0, 3, 6, 9 and 12 was conducted for the purpose of boosting the CTLs infiltration in tumor, which was combined with 3-round intraperitoneal injection of PD-L1 antibody on day 6, 9 and 12 (Fig. S6a). The results showed that

Akk-OMV or PD-L1 antibody treatment alone did not significantly reduced the tumor volume comparing with the control group at the endpoint of tumor growth on day 21, while the tumor volume was significantly reduced after combination treatment of Akk-OMV and PD-L1 antibody on day 15, 18 and 21. Moreover, there was a significant difference of tumor volume between Akk-OMV and combination treatment on day 15 (Fig. S6b). The flow cytometry analysis confirmed that both Akk-OMV and combination treatment significantly increased the intratumoral infiltration of CTLs comparing with the control group, while PD-L1 antibody treatment did not (Fig. S6c). Taken together, these results demonstrated that Akk-OMV activated DC maturation and CTL response, and exhibited the synergistically therapeutic potential with PD-L1 antibody.

3.2. Akk-OMV exhibits a favorable safety profile

Owing to the high density of pathogen-associated molecular patterns (PAMPs), bacteria OMVs have been developed as versatilely self-adjuncting vehicles to improve the immunogenicity of tumor antigens and achieve the therapeutic cancer vaccination [26,31]. However, the lipopolysaccharide and other toxins in OMVs become the major cause of severe toxic effects including cytokine storm and sepsis, hampering the further clinical applications [32]. Given the safety and efficacy of *Akkermansia muciniphila* in various mouse models and in human trials [33,34], we assumed the favorable safety profile of Akk-OMV. Since *Escherichia coli*-derived OMVs were previously found to cause severe toxicity in vivo [35], DH5 α -OMV was chosen as the positive control. After single-dose intraperitoneal injection of Akk-OMV and DH5 α -OMV to BALB/c mice, the serum and major organs were collected for evaluating the liver and renal function and organ histological changes at 8 h post injection (Fig. S7a). There were no obvious histological changes of major organs and statistical differences of liver and renal function indexes between the groups of Akk-OMV and the PBS control, while the serum concentrations of liver enzymes alanine transaminase (ALT), aspartate aminotransferase (AST) and renal function marker blood urea nitrogen (BUN) in DH5 α -OMV vaccinated mice were significantly increased (Figs. S7b–c). We next performed intraperitoneal injection of Akk-OMV and DH5 α -OMV to BALB/c mice every 3 days for 3 times (Fig. 2a). DH5 α -OMV caused 50 % death rate of mice at the endpoint on day 14 (Fig. 2b), and remaining mice displayed visible splenomegaly (Fig. 2c). There were significant differences in serum concentrations of liver albumin (ALB) and total bile acid (TBA) and renal BUN between the groups of DH5 α -OMV and control (Fig. 2d), and hematoxylin & eosin (H&E) staining showed obvious lymphatic nodule disappear and lymphocyte diffuse hyperplasia (Fig. 2e). In addition, Akk-OMV and DH5 α -OMV were subcutaneously injected to C57BL/6 mice at 3 day-intervals for 3 times (Fig. 2f). DH5 α -OMV treatment resulted in the obvious skin damage at the injection site, while mice received Akk-OMV treatment remained similar with the PBS control group (Fig. 2g). H&E staining also indicated the disappear of lymphatic nodules and diffuse hyperplasia of lymphocytes in DH5 α -OMV treated mice (Fig. 2h), and the serum concentrations of liver alkaline phosphatase (ALP), ALB, direct bilirubin (DBIL) and total bilirubin (TBIL) and renal BUN and creatinine (CREA) were significantly increased compared to the control group (Fig. 2i). On the contrary, the major organ histomorphology and biochemical indexes of mice received 3-round intraperitoneal or subcutaneous injection of Akk-OMV

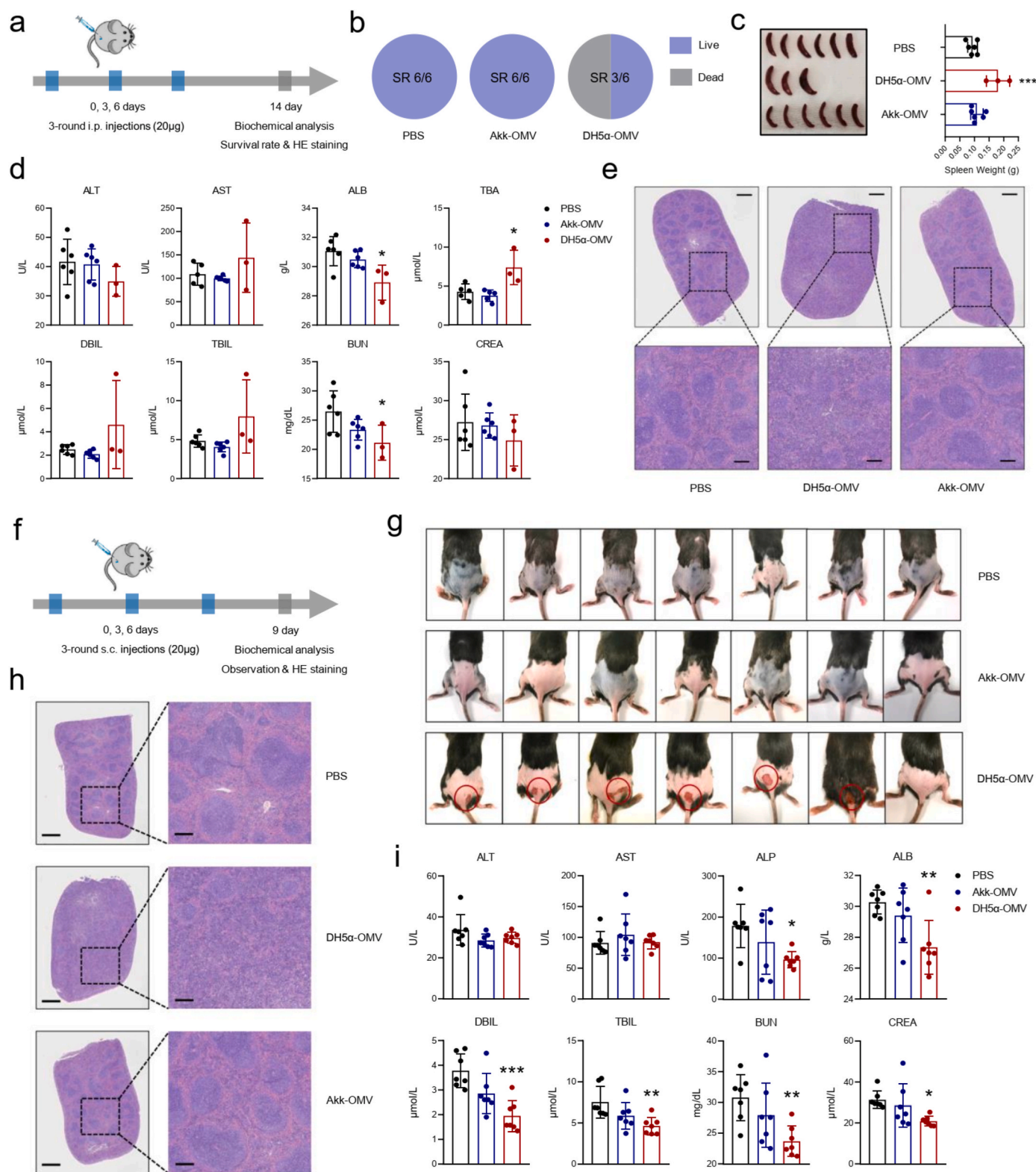


Fig. 2. Akk-OMV exhibited a favorable safety profile over *E. Coli* DH5α-OMV. (a) Experimental design for toxicity evaluation upon 3-round intraperitoneal injection. BALB/c mice were injected with Akk-OMV and DH5α-OMV (20 μg) on day 0, 3 and 6, and were euthanized on day 14. (b) Survival rate of each group at the end point (n = 6). (c) Spleen images and weights at the endpoint (n = 3 and 6). (d) Serum concentrations of hepatic and renal function indexes (n = 3 and 6). (e) Representative H&E staining images of spleens (Scale bar: upper images 1 mm, lower images 250 μm). (f) Experimental design for toxicity evaluation upon subcutaneous injection. C57BL/6 mice were injected at the tail base with Akk-OMV and DH5α-OMV (20 μg) on day 0, 3, 6, and were euthanized on day 9. (g) Skin damage images of different groups at endpoint (n = 7). The skin damage at the injection site was marked by red circle. (h) Representative H&E staining images of spleens (Scale bar: left images 1 mm, right images 250 μm). (i) Serum concentrations of hepatic and renal function indexes (n = 7). Data are presented as mean ± SD. Statistical significance was calculated via one-way ANOVA with Tukey multiple comparisons test. * $p < 0.05$, ** $p < 0.01$, *** $p < 0.001$ versus corresponding control group. (For interpretation of the references to color in this figure legend, the reader is referred to the Web version of this article.)

remained similar with the control group. Collectively, these results demonstrated the favorable safety profile of Akk-OMV, revealing the further application potential for adjuvant immunotherapy strategies.

3.3. Preparation and characterization of Lipo@HEV

The triple vesicle-based hybrid system of Lipo@HEV was fabricated by fusing cationic liposome with tumor cell-derived exosome and Akk-

OMV. Similar to the isolation process of bacterial OMVs, the tumor cell-derived exosomes were enriched by differential centrifugation, and cationic liposomes were prepared using a thin-film hydration method. Then Lipo@HEV was generated by fusing eukaryotic-prokaryotic EVs with cationic liposome through the sonication and co-extrusion procedure. For the characterization study, the TEM images showed that the 4T1, B16-F10 and CT26 tumor cells-derived exosomes and Akk-OMV displayed the nano-sized lipid-bilayer vesicular structure with slightly

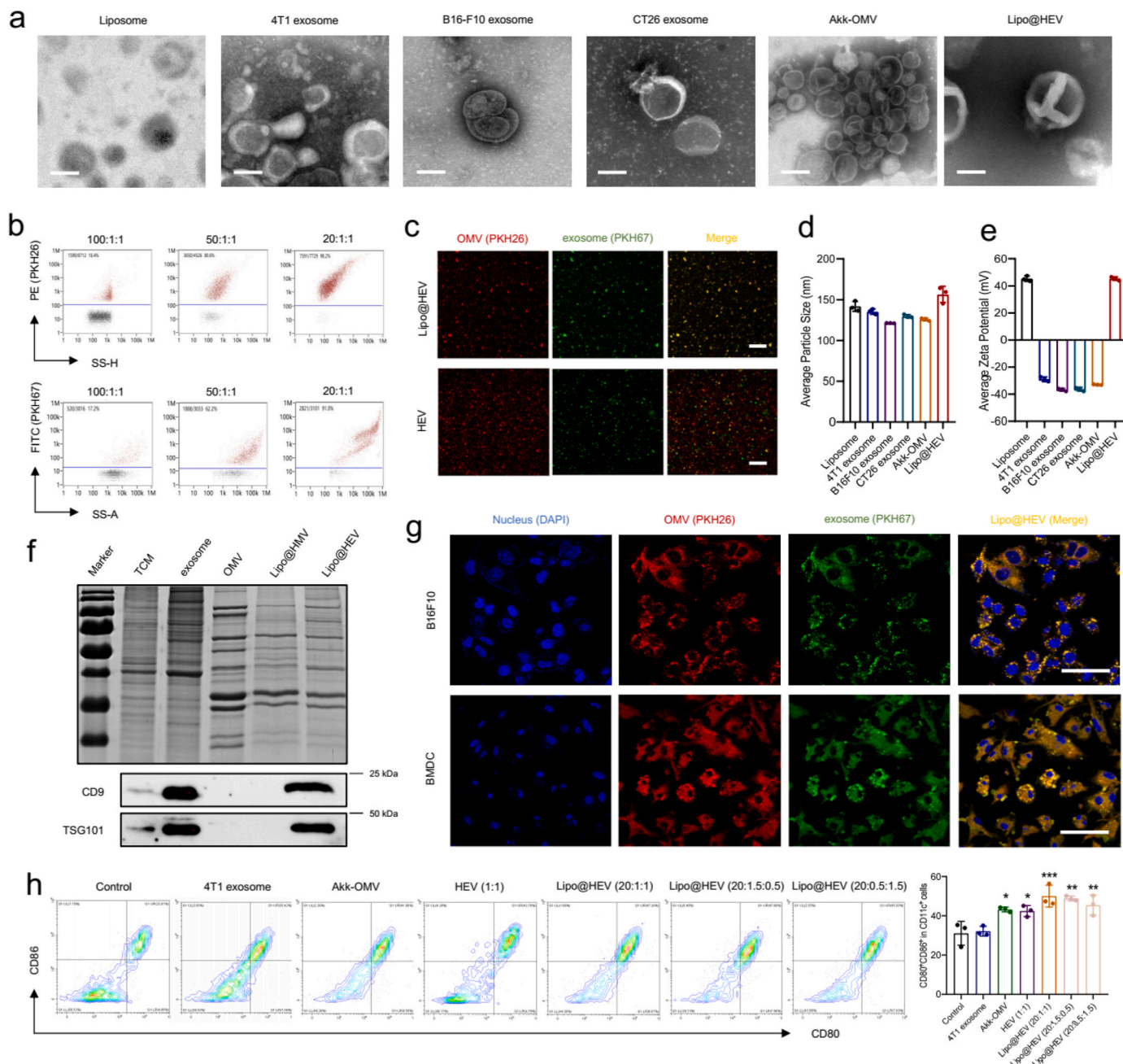


Fig. 3. Preparation and characterization of Lipo@HEV. (a) TEM images of liposome, 4T1 exosome, B16-F10 exosome, CT26 exosome, Akk-OMV and Lipo@HEV (scale bar: 100 nm). (b) Nano-flow cytometry analysis of vesicle fusion in Lipo@HEV prepared at weight ratios of 100:1:1, 50:1:1, 20:1:1, with PKH26-labeled OMV and PKH67-labeled exosome. (c) Representative images of vesicle fusion in Lipo@HEV and HEV via confocal laser scanning microscopy (CLSM) (scale bar: 10 μ m, OMV labeled with PKH26, exosome labeled with PKH67). (d) Particle sizes and (e) zeta potentials of liposome, 4T1 exosome, B16-F10 exosome, Akk-OMV and Lipo@HEV measured by NTA ($n = 3$). (f) SDS-PAGE of protein components and Western blot of exosome markers (CD9 and TSG101) in tumor cell membrane (TCM), exosome, OMV, Lipo@HMV and Lipo@HEV. (g) Colocalization of PKH26/PKH67-labeled Lipo@HEV in B16-F10 cells and BMDCs via CLSM (scale bar: 50 μ m). (h) Flow cytometry images and analysis of DC maturation markers in BMDCs (CD80⁺CD86⁺ in CD11c⁺) after incubation with exosome, OMV, HEV and different formulations of Lipo@HEV for 24 h ($n = 3$). Data are presented as mean \pm SD. Statistical significance was calculated via one-way ANOVA with Tukey multiple comparisons test. * $p < 0.05$, ** $p < 0.01$, *** $p < 0.001$ versus corresponding control group.

different diameters, and Lipo@HEV preserved the vesicular structure after fusion process (Fig. 3a). To verify the vesicle fusion among cationic liposome and different EVs, OMV and exosome were first labeled with a pair of fluorescent dyes PKH26/PKH67, followed by co-fusion with cationic liposome. The nano-flow cytometry analysis indicated that the vesicle fusion was enhanced with increasing amounts of PKH26/PKH67-labeled EVs (100:1:1, 50:1:1, 20:1:1), and the fusion rates at weight ratio of 20:1:1 were 98.2 % (PKH26, PE channel) and 91.0 % (PKH67, FITC channel), respectively, which demonstrated the successful integration of EVs into cationic liposome (Fig. 3b). The vesicle fusion was also visualized via confocal laser scanning microscope (CLSM), while the fusion outcome of hybrid EVs (HEV) using exosome and OMV was unsatisfactory due to the lack of electrostatic adsorptions between cationic liposome and EVs (Fig. 3c), which suggested the necessity of cationic liposome as the co-fusion vector. The NTA results indicated that the average diameters of cationic liposome, exosomes and Akk-OMV ranged from 121.2 ± 0.23 nm to 141.8 ± 6.2 nm, and Lipo@HEV exhibited the slightly increased diameter of 156.3 ± 9.9 nm (Fig. 3d). The average zeta potentials of cationic liposome, 4T1 exosome, B16-F10 exosome and Akk-OMV were 45.3 ± 2.0 mV, -32.0 ± 2.8 mV, -42.7 ± 4.7 mV and -44.7 ± 1.7 mV, respectively, and Lipo@HEV remained the positive surface potential of 45.4 ± 1.3 mV after vesicle fusion (Fig. 3e). Since Lipo@HEV was fabricated to integrate the antigen and adjuvant from EVs, the protein profile was analyzed by SDS-PAGE. The obvious differences in protein compositions between exosome and OMV were observed, and Lipo@HEV resembled a combination of proteins from these EVs. Western blot analysis confirmed that Lipo@HEV contained the exosome markers of CD9 and TSG101 [36], while the hybrid product of tumor cell membrane (TCM) with cationic liposome and OMV (Lipo@HMV) did not (Fig. 3f).

Before we investigated the cellular uptake of Lipo@HEV, no obvious cytotoxicity in B16-F10 and DC2.4 cells was confirmed by CCK8 assay (Fig. S8). The samples of OMV and exosome were labeled with PKH26 and PKH67, respectively, and the PKH26/PKH67 dual-labeling Lipo@HEV was prepared through sonication and extrusion. The internalization of Lipo@HEV into different cell types of B16-F10, DC2.4 and bone marrow-derived DCs (BMDC) was visualized via CLSM after 6 h of incubation (Fig. 3g, and Fig. S9), and flow cytometry analysis showed that the cellular uptake rate of B16-F10 and BMDC was 96.3 % and 94.5 %, respectively (Fig. S10). Since BMDC displays abundant pattern recognition receptors (PRPs) to facilitate the recognition of PAMPs on the surface of OMV originated from the parent bacterial outer membrane [37,38], the cellular uptake of Lipo@HEV by BMDC might be enhanced via hybridized fabrication of cationic liposome with OMV. Similar with OMV, exosome can be internalized into recipient cells via various mechanisms, including phagocytosis, micropinocytosis, membrane fusion, and lipid raft- or receptor-mediated endocytosis [39,40]. Previous study showed that tumor-derived exosome endowed hybrid lipid nanovesicles with homing targeting ability primarily through heparan sulfate proteoglycan (HSPG)-mediated pathway, and the hybrid lipid nanovesicles boosted the nucleic acids delivery through the Golgi and endoplasmic reticulum intracellular freeway transportation, which could bypass the endosome-lysosome degradation pathway [41]. Tumor-derived exosome-liposome hybrid nanoparticles with surface modification of cRGD could enter the target cells through clathrin- and caveolae-mediated endocytosis [42]. In the present study, we fabricated the hybrid lipid nanovesicles with positive surface charge by fusing tumor-derived exosome and OMV with cationic liposome, which was more likely to bind to the target cell membrane with negative surface charge, resulting in the efficient cellular uptake of Lipo@HEV.

We further examine the ability of Lipo@HEV on activating DC maturation in vitro. BMDCs were treated with different EVs and formulations of Lipo@HEV. Flow cytometry analysis showed that the DC maturation was markedly activated in all Akk-OMV containing formulations, while 4T1 tumor cell-derived exosome failed to activate DCs. These results demonstrated that Lipo@HEV inherited the capacity of

promoting DC maturation from Akk-OMV. In addition, Lipo@HEV prepared at the weight ratio of 20:1:1 exhibited the optimal effect on activating DCs (Fig. 3i), which was chosen for further in vivo studies.

3.4. Prophylactic vaccination capacity of Lipo@HEV

To evaluate the vaccination capacity of Lipo@HEV for preventing tumorigenesis, C57BL/6 mice were subcutaneously injected with different formulations at equivalent dose of 40 μ g EV before B16-F10 tumor inoculation (Fig. 4a). The tumor growth curve showed that vaccination of homologous exosome hybrid lipid nanovesicles (Lipo@B16-EXO) slowed the tumor growth, revealing that tumor cell-derived exosome potentiated the hybrid formulation with tumor-preventing capacity by providing the tumor antigens. The Akk-OMV hybrid lipid nanovesicles (Lipo@Akk-OMV) also exhibited the tumor-preventing capacity, which was consistent with our findings of prophylactic antitumor efficacy of Akk-OMV described above. In addition, the homologous tumor exosome and Akk-OMV hybrid lipid nanovesicles (Lipo@B16-HEV) significantly inhibited tumor growth, while the tumor-preventing effect of heterogenous hybrid formulation (Lipo@4T1-HEV) was not obvious, which verified the antigen-specific response induced by Lipo@B16-HEV hybridized with homologous tumor antigens from B16-F10 exosome (Fig. 4b). To gain further insight into the tumor-preventing capacity of Lipo@B16-HEV, we conducted single-cell RNA-sequencing to analyze the cell subsets and DEGs in the pooled tumor samples. After uniform manifold approximation and projection (UMAP) dimension reduction and cell subset marker profiling (Fig. 4c), different cell subsets including melanoma cells, fibroblasts, endothelial cells, macrophages, erythrocytes, granulocytes and B cells were identified (Fig. 4d). The percentages of cell subsets indicated the majority of different melanoma cell subsets (C0-C10), with a minority of fibroblasts (C11), endothelial cells (C12), macrophages (C13), erythrocytes (C14), granulocytes (C15) and B cells (C16) (Fig. 4e). Then we focused on the Hallmark pathway enrichment analysis of DEGs in the melanoma cell subsets, and found higher percentage of cell subset (C0) enriched in the pathway of interferon α and γ response after Lipo@B16-HEV vaccination, while the cell subset (C2) enriched in the hypoxia and glycolysis pathways was decreased (Fig. 4f), implying that Lipo@B16-HEV vaccination maintained the sensitivity of melanoma cells to T cell-mediated immune response [43,44], and altered the hypoxia and metabolic microenvironment. Given the crucial role of immune memory responses in tumor prophylaxis [24], we investigated the splenic TEM cells by flow cytometry. As expected, different hybrid formulations caused enhanced differentiation of TEM cells compared to the control group, and the optimal effect was observed in Lipo@B16-HEV vaccinated mice (Fig. 4g). In summary, these results demonstrated that Lipo@B16-HEV initiated antigen-specific immunity and effectively prevented tumorigenesis through enhanced differentiation of TEM cells.

3.5. Lipo@HEV promotes DC maturation in lymph node and activates CTL response against tumor growth

Motivated by the prophylactic vaccination capacity of Lipo@HEV, we next investigated the antitumor performance and mechanism after tumor inoculation. BALB/c and C57BL/6 mice were first challenged with CT26 and B16-F10 tumor cells on day 0, respectively, and subcutaneous injections of different vaccine formulations began on day 4 at 3 day-intervals for 3 times (Fig. 5a). In CT26 tumor model, the tumor volume and weight were significantly decreased in all treatment groups comparing with the control group, and Lipo@HEV exhibited the optimal effect (Fig. 5b). In B16-F10 tumor model, Lipo@HEV treatment suppressed the tumor growth and weight, while the efficacy of Lipo@B16-EXO or Lipo@Akk-OMV treatment was not obvious (Fig. 5c). To investigate whether Lipo@HEV can accumulate into lymph node for downstream activation of DC maturation and CTL response [45], the DiR-labeled Lipo@HEV, Lipo@Akk-OMV and Lipo@B16-EXO were

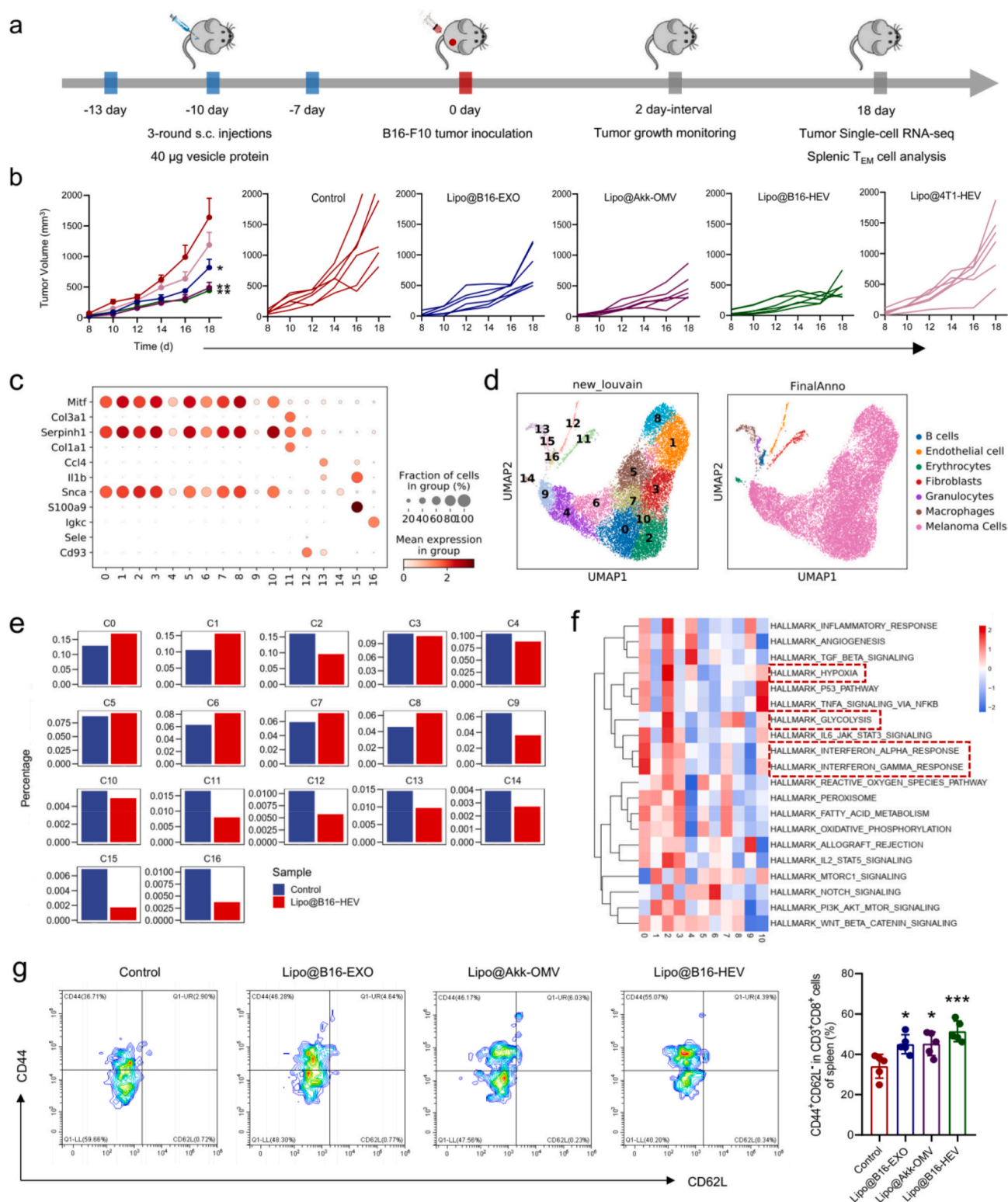


Fig. 4. Prophylactic vaccination efficacy of Lipo@HEV. **(a)** Experimental design: C57BL/6 mice were subcutaneously injected at the tail base with PBS, Lipo@B16-EXO, Lipo@Akk-OMV, Lipo@B16-HEV and Lipo@4T1-HEV (40 μg vesicle protein) on day -13, -10 and -7, followed by inoculation with 2×10^5 B16-F10 cells on day 0. Mice were euthanized on day 18 for single-cell RNA-sequencing in tumors and T_{EM} analysis in spleens. **(b)** Tumor growth kinetics after vaccination of different formulations ($n = 6$). Data are presented as mean \pm SEM. **(c)** Cell markers profiling of defined cell subsets. **(d)** Uniform manifold approximation and projection (UMAP) plot of cells colored by cell types. **(e)** Percentages of different identified cell subsets (C0–C10, melanoma cell subsets; C11, fibroblasts; C12, endothelial cells; C13, macrophages; C14, erythrocytes; C15, granulocytes; C16, B cells). **(f)** Hallmark pathway enrichment analysis of DEGs in melanoma cell subsets. **(g)** Flow cytometry analysis of T_{EM} (CD44⁺CD62L⁻ in CD3⁺CD8⁺) in spleens ($n = 5$). Data are presented as mean \pm SD. Statistical significance was calculated via one-way ANOVA with Tukey multiple comparisons test. * $p < 0.05$, ** $p < 0.01$, *** $p < 0.001$ versus corresponding control group.

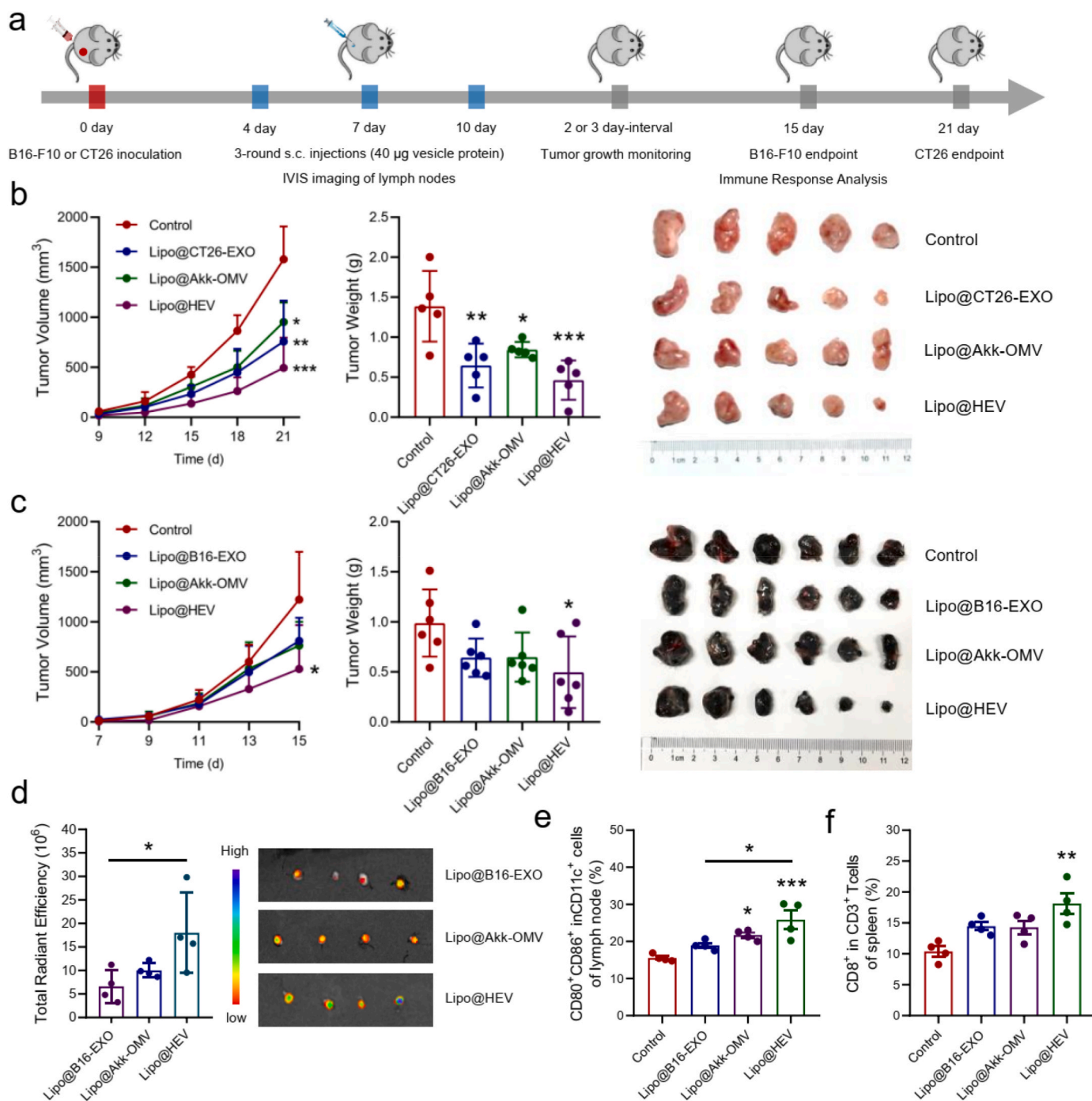


Fig. 5. Lipo@HEV promoted DC maturation in lymph node and activated CTL response against tumor growth. (a) Experimental design: C57BL/6 and BALB/c mice were inoculated with 2×10^5 B16-F10 and CT26 tumor cells on day 0, respectively, and were subcutaneously injected (40 µg vesicle protein) at the tail base with different vaccine formulations on day 4, 7 and 10. The DiR-labeled B16-F10 exosome and Akk-OMV were co-extruded with liposome to generate different DiR-labeled formulations, and C57BL/6 mice were subcutaneously injected at the tail base on day 4. The IVIS imaging was performed at 48 h post-injection. (b) Tumor growth kinetics, tumor weight and images after different treatments of control, Lipo@CT26-EXO, Lipo@Akk-OMV and Lipo@HEV ($n = 5$). (c) Tumor growth kinetics, tumor weight and images after different treatments of control, Lipo@B16-EXO, Lipo@Akk-OMV and Lipo@HEV ($n = 6$). (d) The fluorescence imaging and radiant efficiency of inguinal lymph nodes in different formulation groups ($n = 4$). (e) Flow cytometry analysis of DC maturation ($CD80^+CD86^+$ in $CD11c^+$) of lymph nodes, (f) $CD8^+$ in $CD3^+$ T cells of spleens ($n = 4$). Data are presented as mean \pm SD. Statistical significance was calculated via one-way ANOVA with Tukey multiple comparisons test. * $p < 0.05$, ** $p < 0.01$, *** $p < 0.001$ versus corresponding control group.

subcutaneously injected to C57BL/6 mice on day 4 after tumor inoculation, respectively. The fluorescent signals of inguinal lymph nodes were observed in the different treatment groups at 48 h post-injection, and the fluorescence signals in Lipo@HEV group was almost 3 times higher than those in Lipo@B16-EXO group (Fig. 5d), implying that the integration of adjuvant components from Akk-OMV enhanced the

migration of Lipo@HEV into lymph node. We next evaluated the DC maturation in lymph node and splenic CTL response by flow cytometry. The treatment of Lipo@B16-F10 only slightly increased the DC maturation markers in lymph node, while Akk-OMV containing hybrid formulations, consistent with the findings of BMDC activation in vitro, significantly promoted the DC maturation, and the effect of Lipo@HEV

was superior to that of Lipo@B16-EXO (Fig. 5e, Fig. S11a). The flow cytometry analysis also showed that the splenic CTLs were significantly increased after Lipo@HEV treatment (Fig. 5f, Fig. S11b), with moderate increase of TEM cells (Fig. S12). Taken together, these findings demonstrated that the immunogenicity of tumor cell-derived exosome can be further enhanced by the presence of Akk-OMV, and Lipo@HEV initiated the DC maturation in lymph node and CTL response against the tumor growth by co-delivery of tumor antigen and adjuvant.

3.6. Synergistic antitumor immune response induced by lipo-PD-L1@HEV

Successful cancer immunotherapies should focus on the step-wise aspects of cancer-immunity cycle [46]. Nanoparticle-mediated ablative cancer treatments such as radiotherapy, photothermal therapy, chemotherapies and photodynamic therapy, have been proven to trigger the tumor immunogenic cell death (ICD) in situ that makes tumor antigens available for DCs, which represents an attractive strategy to induce cancer vaccine-like functions [47,48]. This in situ vaccine-like nanomedicine strategy is continuously evolving, evidenced by PTEN-mRNA nanoparticle-mediated autophagy and neutrophil camouflaged nanovesicle-mediated pyroptosis [49,50]. In the present study, we have fabricated the Lipo@HEV, as an ex-vivo vaccination strategy [51], for enhancing the immunogenicity and presentation of tumor antigens by co-delivery of tumor cell-derived exosome and Akk-OMV to DCs, thereby strengthening the antigen-specific CTL response. However, as CD8⁺ T cells activated by cancer vaccination have to infiltrate the tumor tissues to recognize and eradicate tumor cells, the immunosuppressive TME can trigger the dysfunction or exhaustion of CD8⁺ T cells. Thus, immune checkpoint blockade and immunomodulatory agents that can overcome the immunosuppressive TME and sensitize the tumor cells with CD8⁺ T cells, provide more chances in tumor elimination. For combination immunotherapies that are tailored to the distinct immune contexts in the TME, synergistic strategy of utilizing ICIs with cancer vaccines has been proposed for immunosuppressed and cold tumors [52, 53]. In addition, systematically injected ICIs may cause severe side effects such as irAEs associated with inflammation and toxicity [8], gene therapy-guided immune checkpoint blockade could be used as an alternative strategy of reversing CTL exhaustion while avoiding the irAEs of systematically injected ICIs. Since cationic liposome composed of the off-the-shelf lipids such as DOTAP and DOTMA can form colloidal stable nanoparticulate lipoplexes with anionic nucleic acid for gene delivery [54], we proposed to load Lipo@HEV with plasmid to achieve the gene therapy-mediated immune checkpoint blockade in TME. In pursuing this strategy, a previously reported PD-L1 trap plasmid encoding the extracellular PD-L1-binding domain of PD-1 in a trimeric form [28,29], was constructed and loaded into Lipo@HEV (Lipo-PD-L1@HEV).

For characterization study, the TEM analysis showed that Lipo-PD-L1@HEV exhibited a nano-sized vesicular structure (Fig. 6a). The NTA results indicated the increased diameter of Lipo-PD-L1@HEV (170.7 ± 1.9 nm) comparing with Lipo-PD-L1 (147.5 ± 5.5 nm) after vesicle fusion process. The zeta potentials of Lipo-PD-L1@HEV and Lipo-PD-L1 were 41.2 ± 6.0 mV and 48.2 ± 0.2 mV, respectively (Fig. 6b), which suggested the forming of colloidal stable nanovesicles with high positive surface charge [54]. The successful vesicle fusion of Lipo-PD-L1@HEV were visualized by CLSM (Fig. S13). In addition, the internalization of Lipo-PD-L1@HEV into B16-F10 and BMDC was confirmed after PKH26/PKH67 labeling and vesicle fusion procedure (Fig. S14), and the flow cytometric analysis showed that cellular uptake rate was 95.6 % and 95.8 %, respectively (Fig. S15).

For in vivo studies, a safer vaccination-like peritumoral injection regime was chosen for Lipo-PD-L1@HEV to avoid tumor hemorrhage of intratumoral injection while penetrate into the tumor peripheral and deep tissues [55]. To investigate the biodistribution of Lipo-PD-L1@HEV, the DiR-labeled Lipo-PD-L1@HEV was peritumorally injected to 4T1 tumor-bearing mice. As expected, the IVIS analysis

indicated that Lipo-PD-L1@HEV was mainly localized in tumor, with a small portion accumulating into lymph node (Fig. 6c-d). In addition, Lipo@HEV loaded with a luciferase-encoding plasmid (Lipo-luciferase@HEV) was peritumorally injected to B16-F10 tumor-bearing mice. The in vivo and ex vivo bioluminescence signals in tumors were detected at 48 h post-injection (Fig. 6e), and no obvious signals of lymph nodes and other major organs were observed (Fig. 6f), which demonstrated that the plasmid transfection was efficiently occurred in tumors. To evaluate the synergistic immune response induced by Lipo-PD-L1@HEV against the established tumor, B16-F10 tumor-bearing mice with initial tumor volumes of 50–100 mm³ were peritumorally injected with Lipo-PD-L1@HEV and Lipo-PD-L1 every 3 days for 3 times (Fig. 6g). The treatment with Lipo-PD-L1 or Lipo-PD-L1@HEV resulted in the remarkable reduction of tumor volumes compared to the control group, suggesting the local expression of PD-L1 trap for blocking the engagements of PD-1 on CTLs with PD-L1 on tumor cells that invalidate T cell-mediated tumor killing [56,57]. Moreover, the tumor inhibition effect of Lipo-PD-L1@HEV was superior to that of Lipo-PD-L1 (Fig. 6h, Fig. S16a), which verified the synergistically therapeutic efficacy of Lipo-PD-L1@HEV. Flow cytometry analysis indicated that the DC maturation and CTLs in lymph nodes were enhanced after Lipo-PD-L1@HEV treatment (Fig. 6i-j, Figs. S17a-b), and intratumoral infiltration of CTLs was increased as well (Fig. 6k, Fig. S17c), demonstrating the DC maturation and CTL response activated by Lipo-PD-L1@HEV based on the EVs hybrid formulation. The Lipo-PD-L1@HEV treatment also caused a moderate decrease of regulatory T cells (T_{reg}, CD25⁺FOXP3⁺ in CD4⁺) in tumors (Fig. S18), and resulted in the markedly upregulated ratio of CTLs and T_{reg} (Fig. 6l), which implied that Lipo-PD-L1@HEV partially reversed the immunosuppressive TME. We further analyzed the serum cytokines of TNF- α , IL-6 and IFN- γ by enzyme-linked immunosorbent assay (ELISA), and the results showed that these cytokines were all increased after Lipo-PD-L1@HEV treatment, while no significant changes were found in Lipo-PD-L1 group compared to the control (Fig. 6m). The double-labelling immunofluorescence analysis was also performed to visualize the T cell markers of CD4 and CD8 in spleens, and the results showed higher densities of splenic CD4⁺ and CD8⁺ T cells in Lipo-PD-L1@HEV treated mice (Fig. S19). The synergistically therapeutic efficacy of Lipo-PD-L1@HEV was further evaluated in 4T1 tumor-bearing mice with initial tumor volumes of 30–50 mm³. The results indicated that Lipo-PD-L1@HEV treatment markedly inhibited the tumor growth, and the effect of Lipo-PD-L1@HEV was superior to that of Lipo-PD-L1 as well (Fig. 6o, Fig. S16b). Moreover, the Lipo-PD-L1@HEV treated mice exhibited prolonged survival compared to the control and Lipo-PD-L1 treated mice, and 25 % of mice in the Lipo-PD-L1@HEV treatment group survived for more than 50 days (Fig. 6p). During the treatment of Lipo-PD-L1@HEV in B16-F10 and 4T1 tumor-bearing mice, there were no significant body weight changes among different groups (Figs. S20a-b), and the H&E staining of major organs from B16-F10 tumor-bearing mice showed no obvious pathological abnormality (Fig. S20c), suggesting that Lipo-PD-L1@HEV treatment did not cause significant toxicity in vivo.

4. Conclusions

In this work, inspired by the robust association of *Akkermansia muciniphila* with favorable antitumor responses of ICIs in both cancer patients and pre-clinical tumor models, we purified the Akk-OMV and demonstrated its antitumor vaccination efficacy with a favorable biosafety profile, which highlighted the application potential of Akk-OMV as a natural and biocompatible self-adjuvanting vesicle for further cancer vaccination and immunotherapy strategies. Utilizing the vesicle fusion technique that potentiated the hybrid vesicles with intrinsic properties from mono-vesicles, we fabricated the cancer vaccine formulation of Lipo@HEV with tumor cell-derived exosome as an antigen source and Akk-OMV as a natural adjuvant. By co-delivery of

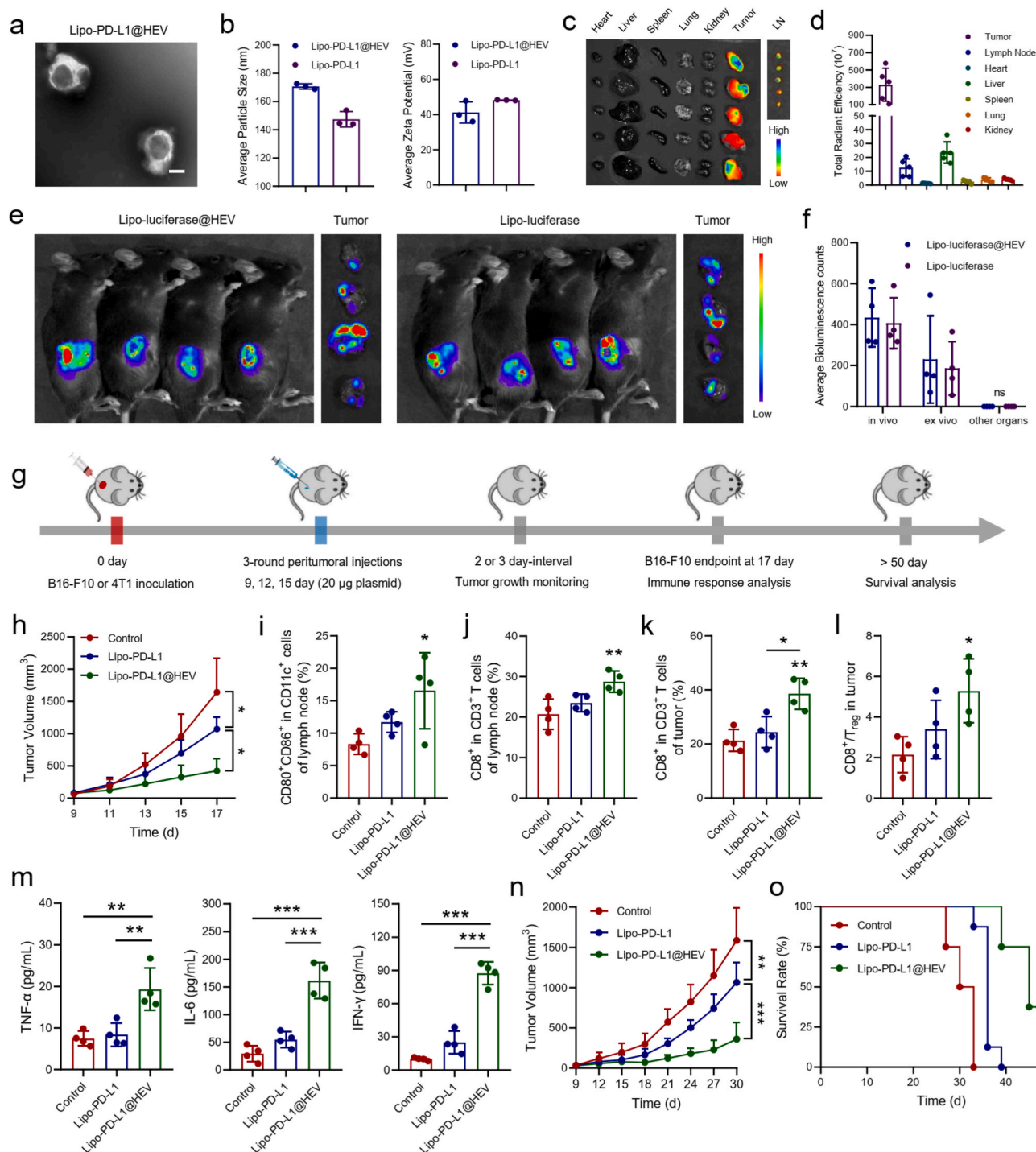


Fig. 6. Fabrication of Lipo-PD-L1@HEV for synergistic antitumor responses against the established tumor. (a) TEM image of Lipo-PD-L1@HEV (scale bar: 100 nm). (b) Average particle sizes and zeta potentials of Lipo-PD-L1@HEV and Lipo-PD-L1 analyzed by NTA ($n = 3$). (c) Fluorescence imaging and (d) total radiant efficiency of tumors, lymph nodes and other major organs at 48 h after peritumoral injection of DiR-labeled Lipo-PD-L1@HEV in 4T1 tumor-bearing mice ($n = 5$). (e) In vivo and ex vivo bioluminescence imaging and (f) average bioluminescence counts of tumors at 48 h after peritumoral injections of Lipo-luciferase@HEV and Lipo-luciferase in B16-F10 tumor-bearing mice ($n = 4$). (g) Experimental design for synergistic antitumor evaluation: C57BL/6 and BALB/c mice were inoculated with 2×10^5 B16-F10 and 4T1 tumor cells on day 0, respectively, followed by peritumoral injections of PBS, Lipo-PD-L1 and Lipo-PD-L1@HEV (20 μ g plasmid) on day 9, 12 and 15. B16-F10 tumor-bearing mice were euthanized on day 17 for immune response analysis, and 4T1 tumor-bearing mice were utilized for tumor growth kinetics and survival rate evaluation. (h) Tumor growth kinetics after different treatments in B16-F10 tumor-bearing mice ($n = 6$). (i) Flow cytometry analysis of DC maturation (CD80⁺CD86⁺ in CD11c⁺) in lymph nodes, (j) CD8⁺ in CD3⁺ T cells in lymph nodes, (k) CD8⁺ in CD3⁺ T cells in tumors, and (l) Ratio of CD8⁺ T cells and T_{reg} cells (CD25⁺FOXP3⁺ in CD4⁺) in tumors ($n = 4$). (m) Serum concentrations of TNF- α , IL-6 and IFN- γ analyzed by ELISA ($n = 4$). (n) Tumor growth kinetics, and (o) survival curves of 4T1 tumor-bearing mice received different treatments of control, Lipo-PD-L1 and Lipo-PD-L1@HEV in 4T1 tumor-bearing mice ($n = 8$). Data are presented as mean \pm SD. Statistical significance was calculated via one-way ANOVA with Tukey multiple comparisons test, and survival rate analysis was calculated by log-rank (Mantel-Cox) test. * $p < 0.05$, ** $p < 0.01$, *** $p < 0.001$ versus corresponding control group.

antigen and adjuvant, Lipo@HEV exhibits the vaccination capacity of inducing memory T cells and preventing tumorigenesis, and exerts therapeutic efficacy by promoting DC maturation in lymph node and activating CTL response. For further achieving the rational combination immunotherapy of cancer vaccination with immune checkpoint blockade, the PD-L1 trap plasmid-loaded Lipo@HEV was fabricated. Upon peritumoral injection, Lipo-PD-L1@HEV localized in tumor to enable the gene therapy-mediated PD-L1 blockade for reversing CTL exhaustion in the TME and avoiding irAEs when delivering PD-L1 antibody systematically. In the meantime, Lipo-PD-L1@HEV penetrated into lymph node to efficiently promote the DC maturation and CTL activation, synergizing with the PD-L1 blocking therapy against the established tumor (Fig. 7). In summary, our work reveals a facile approach and an extensible hybrid lipid nanoplatform by fusing membrane vesicles with plasmid-loaded cationic liposome, providing an attractive strategy for enhanced cancer vaccination and synergistic immunotherapy.

Credit author statement

Q T: Conceptualization, Investigation, Methodology, Data curation, Formal analysis, Validation, Writing - original draft and Writing—review & editing. KX L: Conceptualization, Investigation, Methodology, Data curation, Formal analysis, Validation, Writing - original draft and Writing - review & editing. FW H: Formal analysis, Validation and Writing - review and editing. Y D: Validation and Writing - review and

editing. T Z: Data curation and Validation. MNWE M: Data curation and Validation. ABS A: Data curation and Validation. XY H: Supervision, Project administration, Funding acquisition, Validation and Writing - review and editing.

Ethics approval and consent to participate

All animal experiments were conducted according to all relevant ethical regulations and were approved by the Animal Care and Use Committee of Tongji Hospital, Tongji Medical College, Huazhong University of Science and Technology (SYXK 2019-0106).

Consent for publication

The publication was approved by all the authors.

Declaration of competing interest

The authors declare the following financial interests/personal relationships which may be considered as potential competing interests: Xiaoyuan Huang reports financial support was provided by National Natural Science Foundation of China and Natural Science Foundation of Hubei Province.

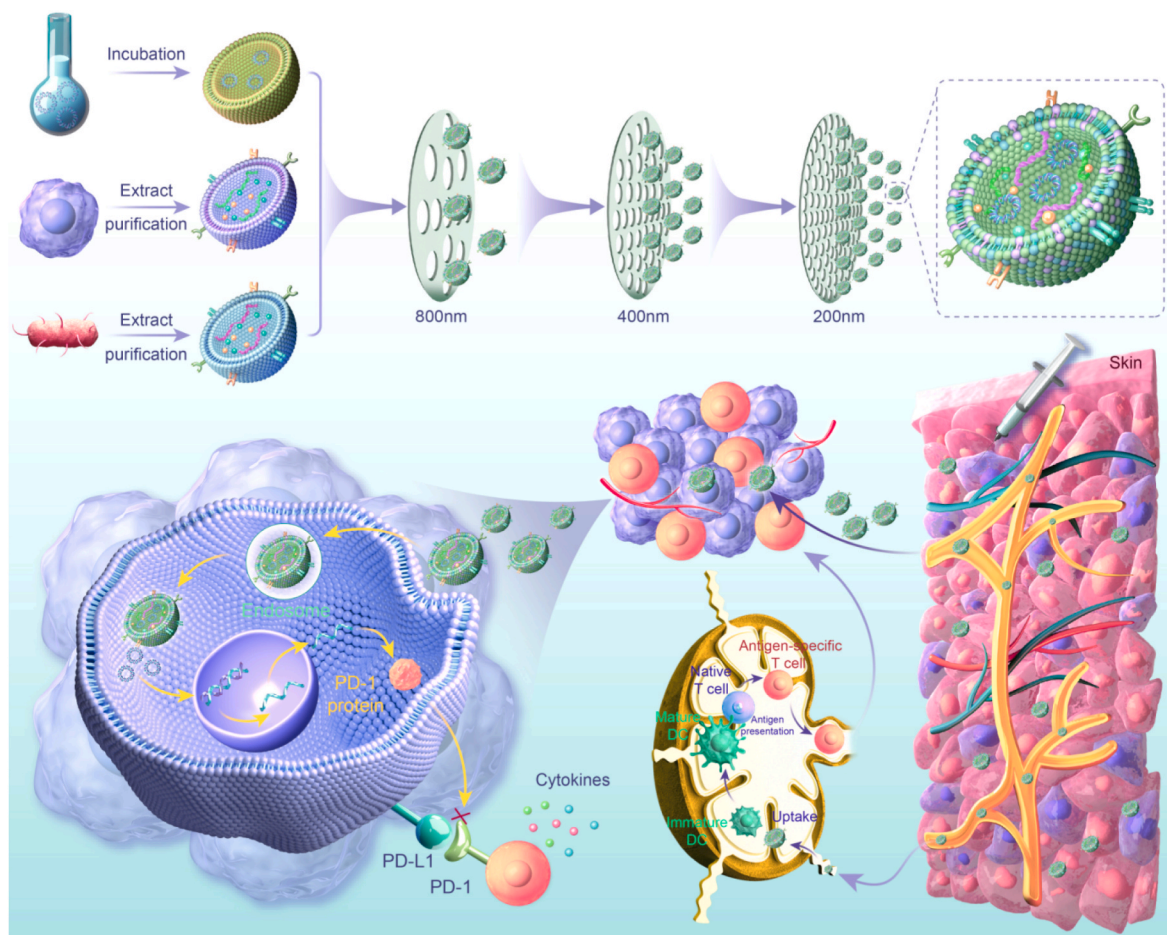


Fig. 7. Schematic illustration of fabricated Lipo-PD-L1@HEV for synergistic cancer immunotherapy. After thin-film hydration of cationic liposome, incubation of cationic liposome with PD-L1 trap plasmid, and purification of tumor cell-derived exosome and Akk-OMV, the Lipo-PD-L1@HEV was fabricated by fusing extracellular vesicles with plasmid-loaded cationic liposome. Upon peritumoral injection, Lipo-PD-L1@HEV can localize in tumor for PD-L1 blockade, and penetrate into lymph node to efficiently initiate DC maturation, antigen presentation and CTL activation, synergistically inhibiting the established tumor.

Data availability

Data will be made available on request.

Funding Acknowledgement

This work was financially supported by the National Natural Science Foundation of China (82004096, 82172717) and Natural Science Foundation of Hubei Province (ZRMS2022000804).

Appendix A. Supplementary data

Supplementary data to this article can be found online at <https://doi.org/10.1016/j.mtbio.2023.100845>.

References

- [1] M. Saxena, S.H. van der Burg, C.J.M. Melief, N. Bhardwaj, Therapeutic cancer vaccines, *Nat. Rev. Cancer* 21 (2021) 360–378.
- [2] M. Platten, L. Bunse, A. Wick, T. Bunse, L. Le Cornet, I. Harting, F. Sahn, K. Sanghvi, C.L. Tan, I. Poschke, et al., A vaccine targeting mutant IDH1 in newly diagnosed glioma, *Nature* 592 (2021) 463–468.
- [3] P.A. Ott, Z. Hu, D.B. Keskin, S.A. Shukla, J. Sun, D.J. Bozym, W. Zhang, A. Luoma, A. Giobbie-Hurder, L. Peter, et al., An immunogenic personal neoantigen vaccine for patients with melanoma, *Nature* 547 (2017) 217–221.
- [4] M.J. Lin, J. Svensson-Arvelund, G.S. Lubitz, A. Marabelle, I. Melero, B.D. Brown, J. D. Brody, Cancer vaccines: the next immunotherapy frontier, *Nat. Can. (Ott.)* 3 (2022) 911–926.
- [5] T. Ye, F. Li, G. Ma, W. Wei, Enhancing therapeutic performance of personalized cancer vaccine via delivery vectors, *Adv. Drug Deliv. Rev.* 177 (2021), 113927.
- [6] L. Hammerich, T.U. Marron, R. Upadhyay, J. Svensson-Arvelund, M. Dhainaut, S. Hussein, Y. Zhan, D. Ostrowski, M. Yellin, H. Marsh, et al., Systemic clinical tumor regressions and potentiation of PD1 blockade with in situ vaccination, *Nat. Med.* 25 (2019) 814–824.
- [7] M. Yarchoan, B.A. Johnson 3rd, E.R. Lutz, D.A. Laheru, E.M. Jaffee, Targeting neoantigens to augment antitumor immunity, *Nat. Rev. Cancer* 17 (2017) 209–222.
- [8] M.A. Postow, R. Sidlow, M.D. Hellmann, Immune-related adverse events associated with immune checkpoint blockade, *N. Engl. J. Med.* 378 (2018) 158–168.
- [9] D.B. Johnson, C.A. Nebhan, J.J. Moslehi, J.M. Balko, Immune-checkpoint inhibitors: long-term implications of toxicity, *Nat. Rev. Clin. Oncol.* 19 (2022) 254–267.
- [10] L.H. Calabrese, C. Calabrese, L.C. Cappelli, Rheumatic immune-related adverse events from cancer immunotherapy, *Nat. Rev. Rheumatol.* 14 (2018) 569–579.
- [11] L. Cheng, A.F. Hill, Therapeutically harnessing extracellular vesicles, *Nat. Rev. Drug Discov.* 21 (2022) 379–399.
- [12] K.S. Park, K. Svennerholm, R. Crescitelli, C. Lässer, I. Gribonika, J. Lötvall, Synthetic bacterial vesicles combined with tumour extracellular vesicles as cancer immunotherapy, *J. Extracell. Vesicles* 10 (2021), e12120.
- [13] B. Routy, V. Gopalakrishnan, R. Daillère, L. Zitvogel, J.A. Wargo, G. Kroemer, The gut microbiota influences anticancer immunosurveillance and general health, *Nat. Rev. Clin. Oncol.* 15 (2018) 382–396.
- [14] V. Matson, J. Fessler, R. Bao, T. Chongsuwan, Y. Zha, M.L. Alegre, J.J. Luke, T. F. Gajewski, The commensal microbiome is associated with anti-PD-1 efficacy in metastatic melanoma patients, *Science* 359 (2018) 104–108.
- [15] B. Routy, E. Le Chatelier, L. Derosa, C.P.M. Duong, M.T. Alou, R. Daillère, A. Fluckiger, M. Messaoudene, C. Rauber, M.P. Roberti, et al., Gut microbiome influences efficacy of PD-1-based immunotherapy against epithelial tumors, *Science* 359 (2018) 91–97.
- [16] L. Derosa, B. Routy, A.M. Thomas, V. Iebba, G. Zalcman, S. Friard, J. Mazieres, C. Audigier-Valette, D. Moro-Sibilot, F. Goldwasser, et al., Intestinal Akkermansia muciniphila predicts clinical response to PD-1 blockade in patients with advanced non-small-cell lung cancer, *Nat. Med.* 28 (2022) 315–324.
- [17] P.D. Cani, C. Depommier, M. Derrien, A. Everard, W.M. de Vos, Akkermansia muciniphila: paradigm for next-generation beneficial microorganisms, *Nat. Rev. Gastroenterol. Hepatol.* 19 (2022) 625–637.
- [18] H.S. Yoon, C.H. Cho, M.S. Yun, S.J. Jang, H.J. You, J.H. Kim, D. Han, K.H. Cha, S. H. Moon, K. Lee, et al., Akkermansia muciniphila secretes a glucagon-like peptide-1-inducing protein that improves glucose homeostasis and ameliorates metabolic disease in mice, *Nat. Microbiol.* 6 (2021) 563–573.
- [19] L. Wang, L. Tang, Y. Feng, S. Zhao, M. Han, C. Zhang, G. Yuan, J. Zhu, S. Cao, Q. Wu, et al., A purified membrane protein from Akkermansia muciniphila or the pasteurized bacterium blunts colitis associated tumorigenesis by modulation of CD8(+) T cells in mice, *Gut* 69 (2020) 1988–1997.
- [20] M. Bae, C.D. Cassilly, X. Liu, S.M. Park, B.K. Tusi, X. Chen, J. Kwon, P. Filipčik, A. S. Bolze, Z. Liu, et al., Akkermansia muciniphila phospholipid induces homeostatic immune responses, *Nature* 608 (2022) 168–173.
- [21] M. Kaparakis-Liaskos, R.L. Ferrero, Immune modulation by bacterial outer membrane vesicles, *Nat. Rev. Immunol.* 15 (2015) 375–387.
- [22] M. Toyofuku, N. Nomura, L. Eberl, Types and origins of bacterial membrane vesicles, *Nat. Rev. Microbiol.* 17 (2019) 13–24.
- [23] N. Krishnan, L.J. Kubiatowicz, M. Holay, J. Zhou, R.H. Fang, L. Zhang, Bacterial membrane vesicles for vaccine applications, *Adv. Drug Deliv. Rev.* 185 (2022), 114294.
- [24] Q. Chen, G. Huang, W. Wu, J. Wang, J. Hu, J. Mao, P.K. Chu, H. Bai, G. Tang, A hybrid eukaryotic-prokaryotic nanoplatform with photothermal modality for enhanced antitumor vaccination, *Adv. Mater.* 32 (2020), e1908185.
- [25] L. Chen, H. Qin, R. Zhao, X. Zhao, L. Lin, Y. Chen, Y. Lin, Y. Li, Y. Qin, Y. Li, et al., Bacterial cytoplasmic membranes synergistically enhance the antitumor activity of autologous cancer vaccines, *Sci. Transl. Med.* 13 (2021).
- [26] K. Cheng, R. Zhao, Y. Li, Y. Qi, Y. Wang, Y. Zhang, H. Qin, Y. Qin, L. Chen, C. Li, et al., Bioengineered bacteria-derived outer membrane vesicles as a versatile antigen display platform for tumor vaccination via Plug-and-Display technology, *Nat. Commun.* 12 (2021) 2041.
- [27] S. Kamerkar, V.S. LeBleu, H. Sugimoto, S. Yang, C.F. Ruivo, S.A. Melo, J.J. Lee, R. Kalluri, Exosomes facilitate therapeutic targeting of oncogenic KRAS in pancreatic cancer, *Nature* 546 (2017) 498–503.
- [28] L. Miao, J. Li, Q. Liu, R. Feng, M. Das, C.M. Lin, T.J. Goodwin, O. Dorosheva, R. Liu, L. Huang, Transient and local expression of chemokine and immune checkpoint traps to treat pancreatic cancer, *ACS Nano* 11 (2017) 8690–8706.
- [29] W. Song, L. Shen, Y. Wang, Q. Liu, T.J. Goodwin, J. Li, O. Dorosheva, T. Liu, R. Liu, L. Huang, Synergistic and low adverse effect cancer immunotherapy by immunogenic chemotherapy and locally expressed PD-L1 trap, *Nat. Commun.* 9 (2018) 2237.
- [30] J. Xu, J. Lv, Q. Zhuang, Z. Yang, Z. Cao, L. Xu, P. Pei, C. Wang, H. Wu, Z. Dong, et al., A general strategy towards personalized nanovaccines based on fluoropolymers for post-surgical cancer immunotherapy, *Nat. Nanotechnol.* 15 (2020) 1043–1052.
- [31] X. Zhao, R. Zhao, G. Nie, Nanocarriers based on bacterial membrane materials for cancer vaccine delivery, *Nat. Protoc.* 17 (2022) 2240–2274.
- [32] C.A. Thaiss, N. Zmora, M. Levy, E. Elinav, The microbiome and innate immunity, *Nature* 535 (2016) 65–74.
- [33] H. Plovier, A. Everard, C. Druart, C. Depommier, M. Van Hul, L. Geurts, J. Chilloux, N. Ottman, T. Duparc, L. Lichtenstein, et al., A purified membrane protein from Akkermansia muciniphila or the pasteurized bacterium improves metabolism in obese and diabetic mice, *Nat. Med.* 23 (2017) 107–113.
- [34] C. Depommier, A. Everard, C. Druart, H. Plovier, M. Van Hul, S. Vieira-Silva, G. Falony, J. Raes, D. Maiter, N.M. Delzenne, et al., Supplementation with Akkermansia muciniphila in overweight and obese human volunteers: a proof-of-concept exploratory study, *Nat. Med.* 25 (2019) 1096–1103.
- [35] S. Qing, C. Lyu, L. Zhu, C. Pan, S. Wang, F. Li, J. Wang, H. Yue, X. Gao, R. Jia, et al., Biomimetic bacterial outer membrane vesicles potentiate safe and efficient tumor microenvironment reprogramming for anticancer therapy, *Adv. Mater.* 32 (2020), e2002085.
- [36] R. Kalluri, V.S. LeBleu, The biology, function, and biomedical applications of exosomes, *Science* 367 (2020), eaau6977.
- [37] M. Bittel, P. Reichert, I. Sarfati, A. Dressel, S. Leikam, S. Uderhardt, I. Stolzer, T. Phu, M. Ng, N. Vu, et al., Visualizing transfer of microbial biomolecules by outer membrane vesicles in microbe-host-communication in vivo, *J. Extracell. Vesicles* 10 (2021), e12159.
- [38] K. Park, K. Svennerholm, R. Crescitelli, C. Lässer, I. Gribonika, J. Lötvall, Synthetic bacterial vesicles combined with tumour extracellular vesicles as cancer immunotherapy, *J. Extracell. Vesicles* 10 (2021), e12120.
- [39] M. Sartorio, E. Pardue, M. Feldman, M. Haurat, Bacterial outer membrane vesicles: from discovery to applications, *Annu. Rev. Microbiol.* 75 (2021) 609–630.
- [40] L. Cheng, A. Hill, Therapeutically harnessing extracellular vesicles, *Nat. Rev. Drug Discov.* 21 (2022) 379–399.
- [41] X. Zhou, Y. Miao, Y. Wang, S. He, L. Guo, J. Mao, M. Chen, Y. Yang, X. Zhang, Y. Gan, Tumour-derived extracellular vesicle membrane hybrid lipid nanovesicles enhance siRNA delivery by tumour-homing and intracellular freeway transportation, *J. Extracell. Vesicles* 11 (2022), e12198.
- [42] L. Li, D. He, Q. Guo, Z. Zhang, D. Ru, L. Wang, K. Gong, F. Liu, Y. Duan, H. Li, Exosome-liposome hybrid nanoparticle codelivery of TP and miR497 conspicuously overcomes chemo-resistant ovarian cancer, *J. Nanobiotechnol.* 20 (2022) 50.
- [43] R.C. Larson, M.C. Kann, S.R. Bailey, N.J. Haradhvala, P.M. Llopis, A.A. Bouffard, I. Scarfó, M.B. Leick, K. Grauwet, T.R. Berger, et al., CAR T cell killing requires the IFN γ pathway in solid but not liquid tumours, *Nature* 604 (2022) 563–570.
- [44] S. Zhong, Q. Li, C. Wen, Y. Li, Y. Zhou, Z. Jin, G. Ye, Y. Zhao, J. Hou, Y. Li, L. Tang, Interferon α facilitates anti-HBV cellular immune response in a B cell-dependent manner, *Antivir. Res.* 207 (2022), 105420.
- [45] N.L. Trevaskis, L.M. Kaminskas, C.J. Porter, From sewer to saviour - targeting the lymphatic system to promote drug exposure and activity, *Nat. Rev. Drug Discov.* 14 (2015) 781–803.
- [46] Q. Li, Z. Shi, F. Zhang, W. Zeng, D. Zhu, L. Mei, Symphony of nanomaterials and immunotherapy based on the cancer-immunity cycle, *Acta Pharm. Sin. B* 12 (2022) 107–134.
- [47] Y. Yi, M. Yu, W. Li, D. Zhu, L. Mei, M. Ou, Vaccine-like nanomedicine for cancer immunotherapy, *J. Contr. Release* 355 (2023) 760–778.
- [48] Y. Yu, Q. Cheng, X. Ji, H. Chen, W. Zeng, X. Zeng, Y. Zhao, L. Mei, Engineered drug-loaded cellular membrane nanovesicles for efficient treatment of postsurgical cancer recurrence and metastasis, *Sci. Adv.* 8 (2022), eadd3599.
- [49] Y. Lin, Y. Wang, J. Ding, A. Jiang, J. Wang, M. Yu, S. Blake, S. Liu, C. Bieberich, O. Farokhzad, et al., Reactivation of the tumor suppressor PTEN by mRNA nanoparticles enhances antitumor immunity in preclinical models, *Sci. Transl. Med.* 13 (2021), eaba9772.

- [50] X. Yu, G. Xing, S. Sheng, L. Jin, Y. Zhang, D. Zhu, L. Mei, X. Dong, F. Lv, Neutrophil camouflaged stealth nanovehicle for photothermal-induced tumor immunotherapy by triggering pyroptosis, *Adv. Sci.* 10 (2023), e2207456.
- [51] M. Lin, J. Svensson-Arvelund, G. Lubitz, A. Marabelle, I. Melero, B. Brown, J. Brody, Cancer vaccines: the next immunotherapy frontier, *Nat. Can.* 3 (2022) 911–926.
- [52] L. Miao, Y. Zhang, L. Huang, mRNA vaccine for cancer immunotherapy, *Mol. Cancer* 20 (2021) 41.
- [53] N. Kirchhammer, M.P. Trefny, P. Auf der Maur, H. Läubli, A. Zippelius, Combination cancer immunotherapies: emerging treatment strategies adapted to the tumor microenvironment, *Sci. Transl. Med.* 14 (2022), eabo3605.
- [54] L.M. Kranz, M. Diken, H. Haas, S. Kreiter, C. Loquai, K.C. Reuter, M. Meng, D. Fritz, F. Vascotto, H. Hefesha, et al., Systemic RNA delivery to dendritic cells exploits antiviral defence for cancer immunotherapy, *Nature* 534 (2016) 396–401.
- [55] L. Zhang, J. Zhao, X. Hu, C. Wang, Y. Jia, C. Zhu, S. Xie, J. Lee, F. Li, D. Ling, A peritumorally injected immunomodulating adjuvant elicits robust and safe metalloimmunotherapy against solid tumors, *Adv. Mater.* 34 (2022), e2206915.
- [56] P. Sharma, J.P. Allison, Immune checkpoint targeting in cancer therapy: toward combination strategies with curative potential, *Cell* 161 (2015) 205–214.
- [57] W. Zou, J.D. Wolchok, L. Chen, PD-L1 (B7-H1) and PD-1 pathway blockade for cancer therapy: mechanisms, response biomarkers, and combinations, *Sci. Transl. Med.* 8 (2016), 328rv324.